Lightning Phenomenology Notes
Note 12
17 August 1984

COMPARISON OF PUBLISHED HEMP AND NATURAL LIGHTNING ON THE SURFACE OF AN AIRCRAFT*

R. L. Gardner
L. Baker
J. L. Gilbert

Mission Research Corporation
1720 Randolph Road, S.E.
Albuquerque, New Mexico 87106

C. E. Baum
D. J. Andersh

Air Force Weapons Laboratory
Kirtland Air Force Base
New Mexico 87117

ABSTRACT

High altitude EMP (HEMP) and its concomitant electromagnetic environment potentially threaten aircraft. HEMP, a short (~0.1 μs) pulse of large amplitude (~50 kV/m) arrives at aircraft essentially as a plane wave. Although this pulse generally contains no oscillations (zero crossings), its Fourier transform shows frequency content over a wide band, with significant content up to 100 MHz. For present purposes we use a well-known public domain HEMP waveform.

Lightning, another potential threat, can interact with an aircraft in two essentially different ways. First, for a nearby strike, the electromagnetic fields generated in and near the stroke channel impinge on the aircraft. Second, for a direct strike on the aircraft, the stroke current actually flows on the conducting structure of the aircraft. The first of these effects may be called field interaction and the second, current injection. It is reasonable to expect that the latter may have larger effects than the former because the strike current path is along the aircraft.

Because of the increasing concerns about these two threats, this study assessed the differences between the electromagnetic environment associated with high altitude EMP (HEMP) and that associated with natural lightning, including the manner in which they affect aircraft.

*Work supported under contract F29601-82-C-0027

The investigation was based on existing data on the currents in lightning strokes from measurements on the ground and from aircraft that had experienced direct strikes. Additional information about the magnitude and pulse shape of the lightning current was inferred by remote sensing of the electromagnetic fields of the lightning channel. Examination of the available data indicates that a reasonable worst case waveform for the lightning discharge current can be described by a maximum current of 10^5 A, a maximum rate of rise of about 10^{11} A/s, and a duration of about 50 μs.

The comparison of HEMP and lightning was accomplished for the electromagnetic environment by using simple models that clearly characterized the salient features of the electromagnetic environments associated with either lightning or HEMP. Analysis of the comparison rendered three regions of the frequency spectrum: below about 1 MHz, the lightning direct strike clearly dominated; above about 10 MHz, HEMP clearly produced larger fields and currents; between those two frequencies, the electromagnetic interaction of the two threats with the aircraft structure is so complex that neither threat clearly dominated.

The consequences of this kind of electromagnetic interference and/or damage will have serious repercussions during wartime. Although exposure to lightning will increase during hostilities; and, although eliminating peacetime rules governing thunderstorm avoidance will concomitantly increase the probability of a lightning strike on or near an aircraft, the actuality of a lightning strike will be significantly less frequent than exposure to HEMP. Indeed during wartime, there is a high probability that an aircraft will be exposed to HEMP.

Data presently show that in 37 percent of reported lightning strikes, after the mishap occurred the pilot made a precautionary landing that prematurely terminated the mission. Such a high failure rate per lightning event is tolerable because the incidence of lightning strikes is low (about 1 per 10^6 flight hours). However, because of the more frequent encounters with HEMP, a similar abort rate would be catastrophic for fleet efficiency during wartime.

CONTENTS

CONTENTS (Concluded)

ILLUSTRATIONS

ILLUSTRATIONS (Continued)

ILLUSTRATIONS (Concluded)

I. INTRODUCTION

Although both HEMP and lightning are threats to aircraft in flight, differences between them occur on several distinct levels of the interaction process. Additionally, the interaction of the external electromagnetic signals with the aircraft's internal electrical systems depends on many factors. Therefore, to make the interaction analysis tractable, the entire process is separated into three approximately independent parts: the external interaction, the mode of penetration to the interior of the aircraft, and the excitation of the elements of the aircraft's internal electrical system. This procedure assumes that the external electromagnetic field is independent of the interior system (that is, the system must be at least partially shielded from the electromagnetic field) and that the mode of penetration is insensitive to the internal components.

Once inside the aircraft, the electromagnetic fields caused either by lightning or HEMP couple to the system's electronics in a similar manner. Consequently, this report discusses the electromagnetic environments that induce currents and charges on the aircraft's surface; it focuses then, on the first level of the interaction process.

As the aircraft's structure interacts with the external environment, currents and charges arise on its surface. This external electromagnetic environment may be generated by the incident fields of HEMP, nearby lightning or by the current injected by direct strike lightning. The electromagnetic energy in these currents and charges may penetrate the aircraft through apertures, through the aircraft skin, by the diffusion of the magnetic fields, or through system electrical cables or other conductors that may penetrate the surface of the aircraft. Once inside, the electromagnetic fields couple to the system's cables and subsequently cause currents at the pins of various electronic boxes where they may damage or upset electronic circuits. This report discusses the electromagnetic environment caused by lightning or HEMP before the penetration to the internal circuits. Field penetration and

interaction with circuits are beyond the scope of this report. These other aspects of the threat do not first order differ between EMP and lightning for a given portion of the frequency spectrum, once the electromagnetic environment is given.

Section II of the report describes the electromagnetic environments generated by HEMP and lightning. For HEMP, this environment is characterized by the waveform of a plane wave incident on the aircraft and its Fourier transform. For lightning, the current conductivity, etc. in the discharge channel characterizes the environment. Since a nearby strike interacts with the aircraft less efficiently than a direct strike since the direct strike current is directly attached to the aircraft, this study concentrated on the direct strike.

The fundamentals of the interaction of the environment with the aircraft are presented in Section III. This section describes the simple geometric and physical models used to characterize the salient features of the interaction of the currents and fields, with the aircraft. Significantly, because these simple models are exclusively linear, they omit the nonlinear behavior of the corona as well as the attached lightning channel. During a lightning strike, the corona enveloping the aircraft may alter the aperture's transmission of electromagnetic signals to the aircraft's interior. The attached channel and aircraft form a nonlinear circuit which, in turn, affects the current in the lightning discharge.

The interaction models, described in Section III, are used to compare lightning and HEMP on the surface of the aircraft, in Section IV. The various interaction models are used to compare HEMP and lightning in several different frequency regimes. These frequency regimes correspond to: the subresonance, or below 1 MHz region; the resonance, or 1-10 MHz region; and the greater than 10 MHz region.

Finally, Section V, discusses the operational considerations deduced from comparing these two threats. During wartime, an aircraft is essentially

certain of being exposed to HEMP at least once during a mission. Lightning, however, normally strikes only in thunderstorms and thunderstorms may be localized geographically and seasonally; consequently during a wartime mission, HEMP is a more probable threat to aircraft than lightning. Therefore, similar mission abort probabilities per event for HEMP and lightning have dissimilar impacts on fleet efficiency. Because of the aircraft's more frequent encounters with EMP, a 37 percent failure probability per event will seriously erode the number of missions successfully completed. Although it is desirable to harden aircraft so that both threats can be minimized, aircraft designed to perform during wartime should be protected against HEMP first so that wartime missions will not be aborted at significant rates.

II. ELECTROMAGNETIC ENVIRONMENTS

This section discusses the electromagnetic environments produced by high altitude EMP (HEMP) and lightning. The HEMP generation mechanism, described first, follows the description for HEMP as an incident plane wave, based on studies of detailed weapon output calculations, with a waveform specified by the Air Force Weapons Laboratory (Ref. 1). Next, the data from measurements of natural lightning are surveyed and a current waveform deduced. The current waveform, a simple function with an analytic Fourier transform, may be used easily by design engineers. This waveform represents natural lightning's characteristics inferred by examining the available data.

1. HIGH ALTITUDE EMP ENVIRONMENTS

High altitude EMP (HEMP), a phenomenon of long duration, is caused by the disturbance of the upper atmosphere by a high altitude nuclear explosion. In this paper, only the first microsecond of the disturbance will be considered. During this time, high energy gamma rays with an average energy of about 1.6 MeV interact with the atmosphere. The affected region will be 20-40 km above the earth because the range of this generation mechanism is limited by line of sight from the weapon to the atmosphere. The effective range for a single nuclear weapon exploded over the central United States is shown in Figure 1. The small circle is for a 100 km height of burst. The large circle is for 500 km height of burst.

During the first microsecond of HEMP generation, the weapon prompt gamma rays Compton scatter electrons from air molecules that are then bent by the earth's magnetic field (Fig. 2). In the early stages of energy production by the nuclear weapon, the gammas are generated and form an outgoing spherical shell traveling at the speed of light. The shell is about 10 m (30 ns of light travel time) thick. Above 50 km altitude, the atmosphere is too thin for the gammas to interact with it. Below 50 km, the Compton electrons form a radial current as the electrons leave the more massive atoms behind.

The outgoing electrons are bent in the earth's magnetic field to a radius of about 80 m as shown schematically in Figure 3. The electrons travel

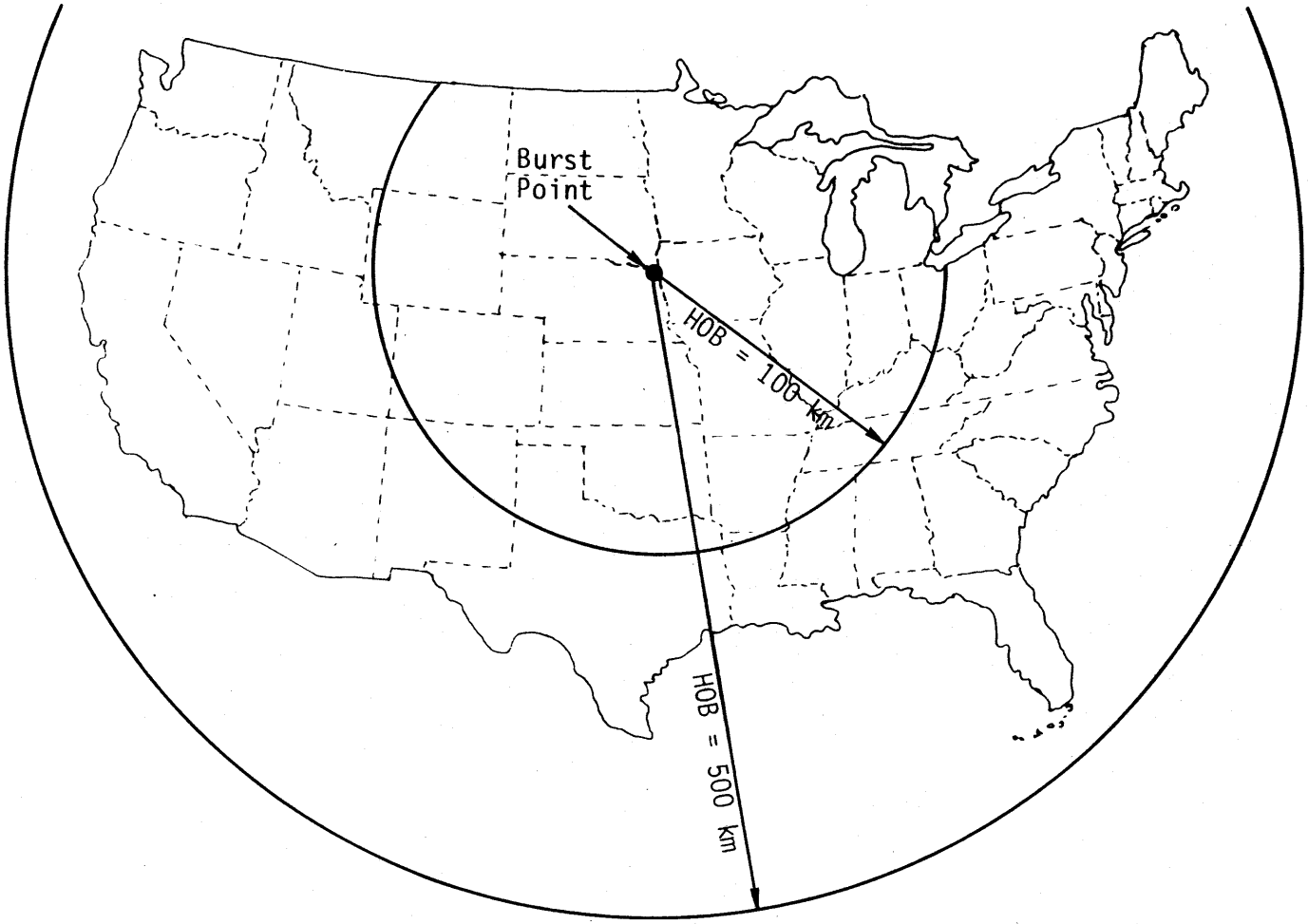

Figure 1. Limits of coverage for height of burst (HOB) at 100 and 500 km located over the central U.S.

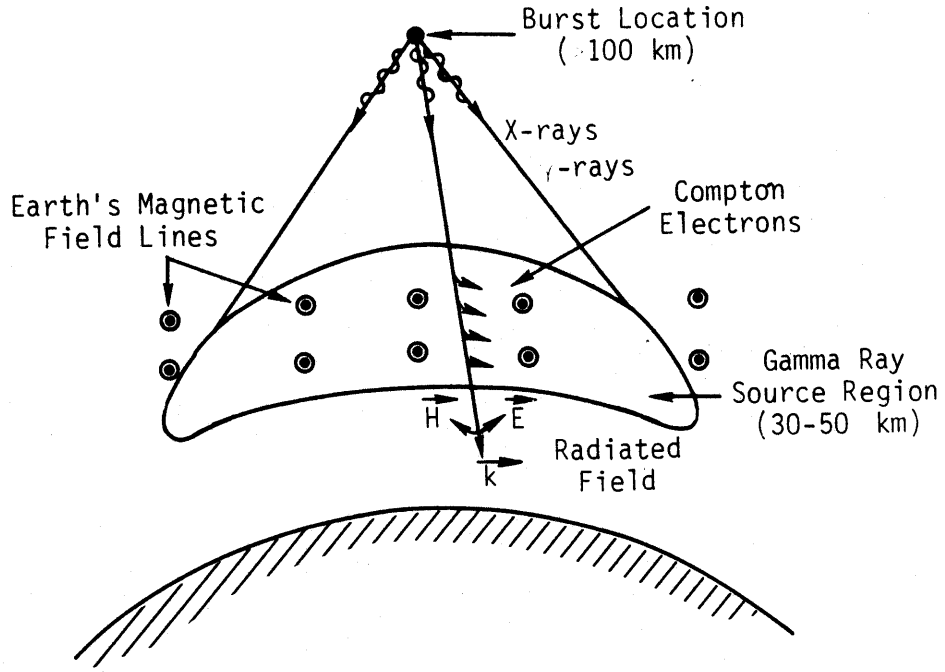

Figure 2. Schematic representation of high-altitude EMP generation (Ref. 2).

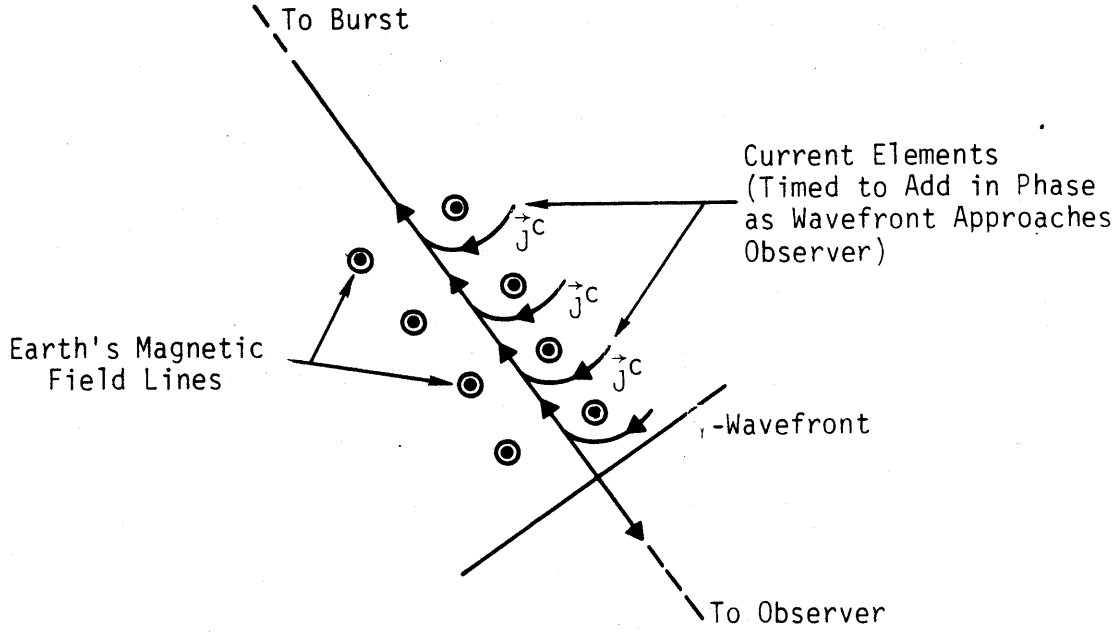

Figure 3. Diagram indicating the current elements due to geomagnetic turning and how they add in-phase to give a large outgoing wave (Ref. 2).

through about 90° of orbit before they are scattered by atoms within the atmosphere. Electrons traveling at such high velocity radiate perpendicularly to the direction of travel; thus when they are bent in the earth's magnetic field, the electrons form a continuum of antennas radiating in phase. Since the outgoing gammas and the HEMP wave are both traveling at the speed of light, the phase of the EMP signal is preserved; consequently the gammas reaching lower levels in the atmosphere reinforce the fields from HEMP generated at higher altitudes. The phase coherence, however, tends to be lost after about 50 ns, thereby limiting the duration of the early time HEMP.

As the Compton electrons travel in the atmosphere, they scatter off of air molecules and atoms. This scattering produces about 30,000 secondary electrons per primary electron. By forming a background conductivity, these electrons eventually limit the peak fields of early time HEMP. The limiting value of the field is known as the saturation field and can be estimated to be about 60 kV/m (Ref. 2). Since the saturation value represents a maximum, it was used in the calculations for comparing HEMP and lightning. Many authors use the value of 50 kV/m in representative, unclassified calculations (Ref. 3).

During the 1962 nuclear test series, some early estimates of high altitude EMP were made in order to set oscilloscopes and other instrumentation to be used for measuring HEMP. These calculations, though, substantially underestimated the peak fields. Consequently, most of the measurements of HEMP from the early, above ground nuclear tests were off-scale. However, there were other more successful measurements; a comparison of one of those measurements with more modern prediction methods is shown in Figure 4.

The CHAP code, whose results are shown in Figure 4 both with and without corrections for instrumentation response, exemplifies modern, sophisticated analysis techniques used to estimate HEMP waveforms for various device types and weapon geometries (Ref. 4). When the uncertainties in the instrumentation response (frequency response, dynamic range, etc.) are considered, agreement of the CHAP prediction, with the instrumentation response folded in, is quite good.

The incident HEMP waveform depends on a number of factors including: height of burst, device type, atmospheric conditions, and distance from the

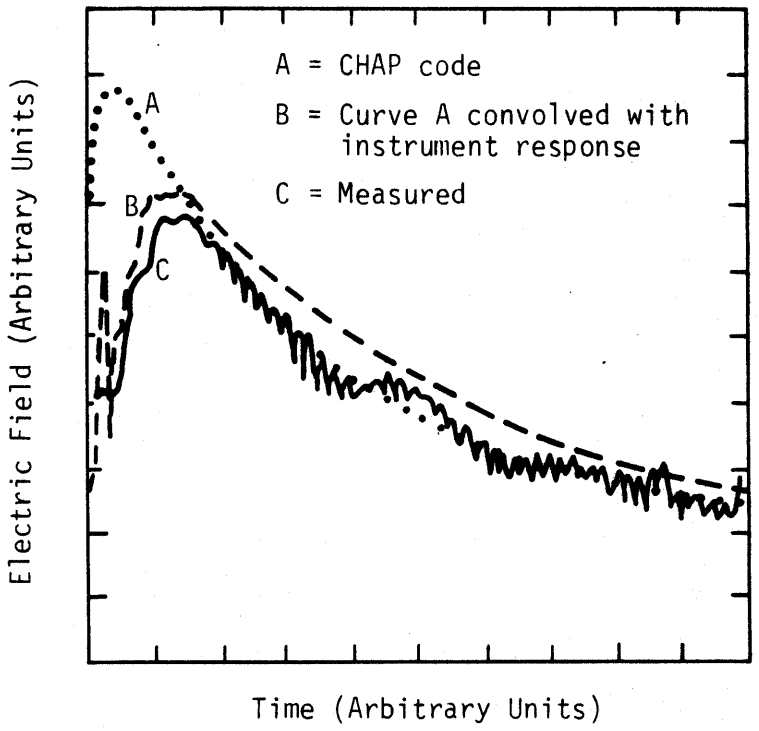

Figure 4. Comparisons of experimental and theoretical EMP waveforms (Ref. 2).

explosion. In the HEMP unclassified literature two waveforms are commonly used to specify the incident waveform. The first is a double exponential (Ref. 1). Although the equations presented here use the saturation field 60 kV/m, 50 kV/m is often used in the other parts of the HEMP literature (Ref. 4). The double exponential waveform is

$$E(t) = E_0\left(e^{-t/\tau_f} - e^{-t/\tau_r}\right) U(t) \qquad (1)$$

where

E_0 = 60 kV/m (saturation field)

τ_f = 250 ns is the fall time constant

τ_r = 2 ns is the rise time constant

and U(t) is unit step function (Ref. 1). These time constants are estimated from an envelope enclosing the results of more complex calculations associated with specific threat scenarios.

The disadvantage of the function shown in Equation 1 is that its derivative is discontinuous at t = 0. Since some interaction processes with aircraft depend on the time derivative of the incident field, a double exponential function may predict non-physical results at early times. An improved waveform without this non-physical behavior of a discontinuity in slope is described by:

$$E(t) = \frac{E_0}{e^{-(t-t_0)/\tau_r} + e^{(t-t_0)/\tau_f}} \qquad (2)$$

Although the function in Equation 2 does have nonzero values at negative times, the error inherent in early time behavior can be made as small as desired by choosing t_0 properly. The variables in Equation 2 have the same values and meanings as those in Equation 1. Plots of Equations 1 and 2 are shown in Figure 5 while Figure 6 shows the plot of the first time derivatives of these two functions. The plots clearly demonstrate the spurious behavior of the slope of the function described by Equation 1. The waveform described by Equation 2 better approximates the early exponential growth of the HEMP incident field. Since the early time weapon gamma flux rises with the weapon energy production, the early time HEMP pulse indeed rises exponentially. In the frequency domain (Fig. 7), this behavior is manifested in the exponential roll-off at high frequency of the Fourier transform of Equation 2 when it is compared with the $1/f^2$ roll-off at high frequency of the transform of Equation 1. The reciprocal double exponential (Eq. 2) better matches the HEMP waveforms calculated for particular weapons using detailed computer models.

In this comparison of HEMP and lightning, HEMP will be treated as an incident plane wave with the waveform described by Equation 2. With this waveform, the peak amplitude is the predicted saturation value of 60 kV/m with rise time constant of 2 ns and a fall time constant of 250 ns.

2. LIGHTNING ENVIRONMENT

In this report, the current, that is the electromagnetic environment for direct and nearby strikes, is assumed to be produced in a return stroke because it typically has the largest currents and rates of rise. Detailed

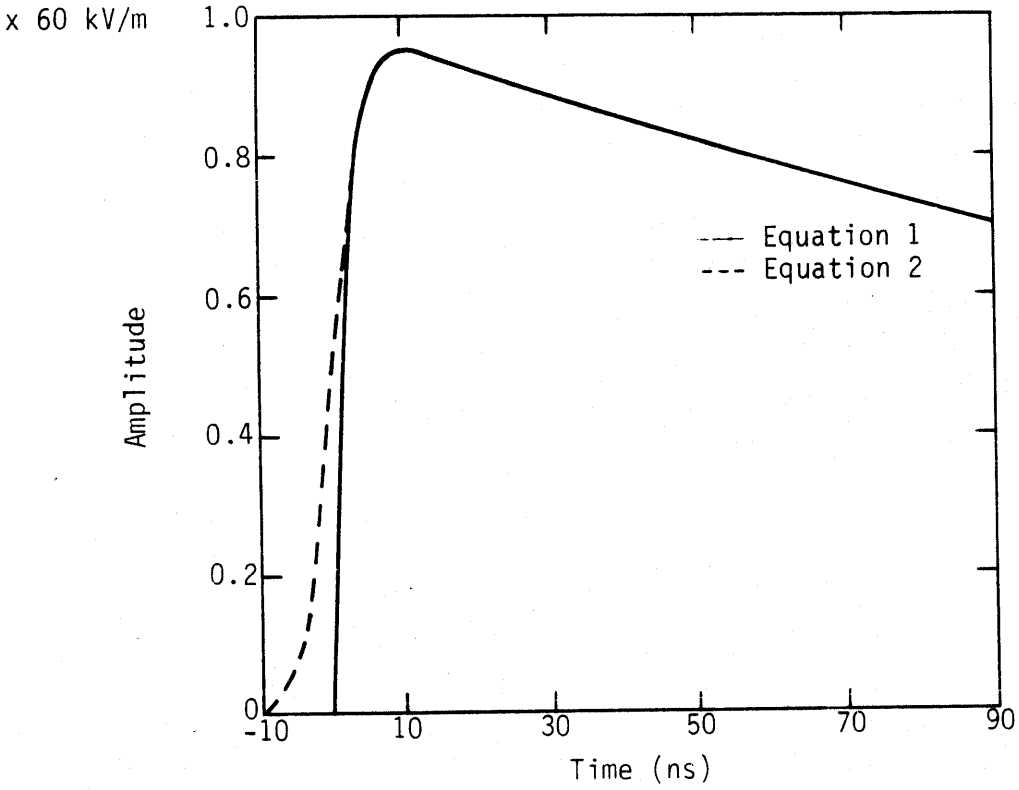

Figure 5. Two canonical HEMP waveforms: τ_r = 2 ns, τ_f = 250 ns, t_0 = 0.

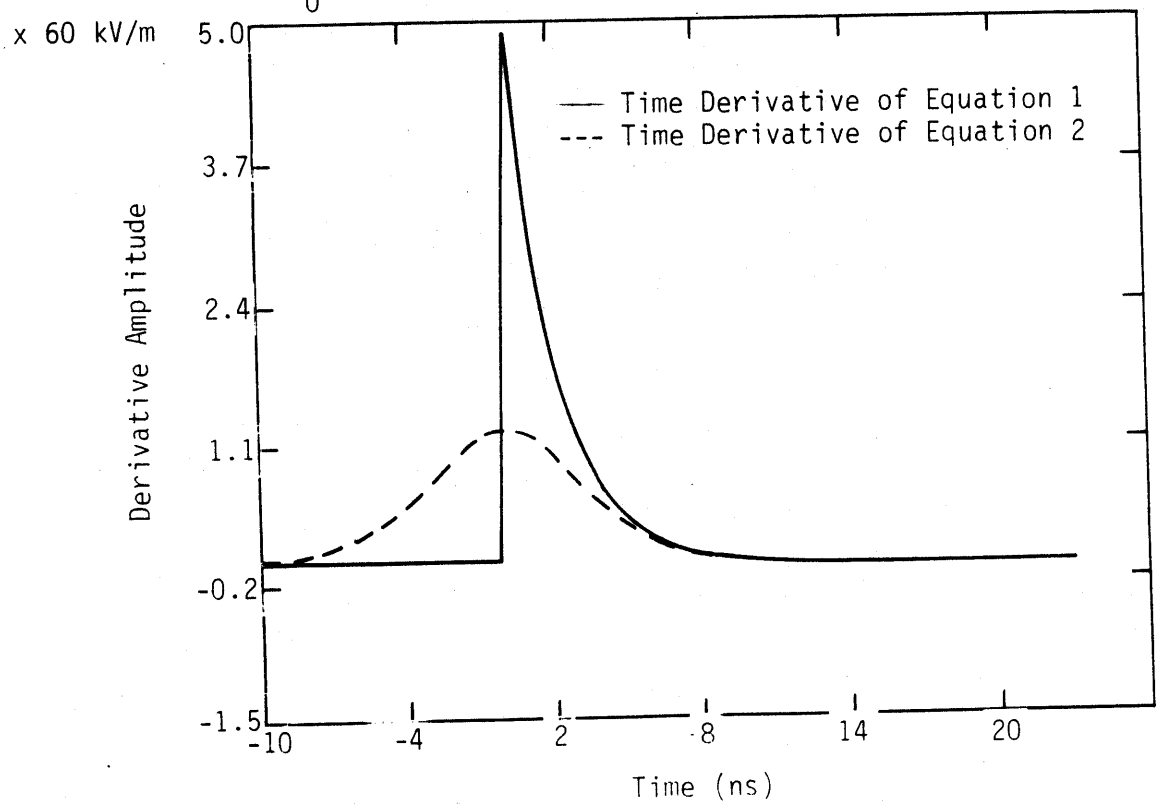

Figure 6. Time derivatives of canonical HEMP waveforms plotted in Figure 5.

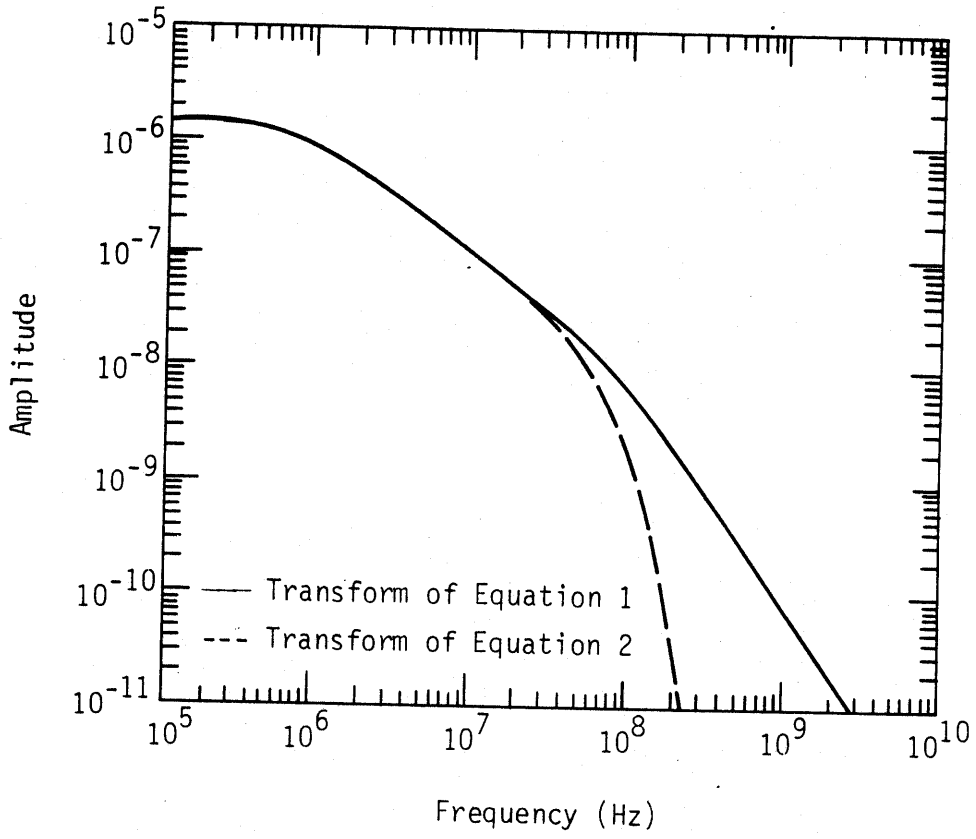

Figure 7. Fourier transform amplitude for the two canonical HEMP waveforms described by Equations 1 and 2.

descriptions of the sequence of events in a lightning discharge and relevant definitions are contained in Uman (Ref. 5) and Golde (Ref. 6). At this time, intracloud events make up the NASA F-106B program's (a program designed to gather data on lightning interaction with aircraft (Ref. 7) data base of strike measurements, and the sequence of these intracloud events is not as clear as the sequence developed for cloud to ground strikes. For the airborne measurements, those currents exceeding the instrumentation trigger threshold are defined as strikes.

The lightning electromagnetic environment, then, consists of the currents in the discharge channel; this channel may include the aircraft. To determine

the complete electromagnetic environment to be used as a threat specification, it is necessary to find the current in an undisturbed lightning channel at aircraft altitudes. Principally, this current is that of the return stroke since the largest peak currents occur in that phase of the lightning discharge; however, the series of fast leader type processes must also be considered.

To characterize the lightning threat, three figures of merit are sufficient to specify either of the double exponential waveforms used for HEMP in Equations 1 and 2. The three figures of merit considered here are:

(1) Peak current
(2) Peak rate of rise of the current
(3) Integral of the pulse

A reciprocal double exponential has these three figures of merit as parameters, is easy to work with, and has an analytic Laplace transform.

Since the detailed theoretical modeling effort applied to HEMP has not been applied to lightning, it was necessary to use empirical techniques to determine the figures of merit listed above. All of the available measurements from which estimates of lightning current parameters are derived may be divided into three classes:

(1) Tower measurements
(2) Measurements on aircraft in flight
(3) Radiated field measurements

Data from each of these sources were used to estimate the current in the lightning channel. This current within the channel establishes the lightning current waveform that constitutes the threat.

a. Tower Measurements--Tower measurements of lightning currents are made using current sensors installed on metal towers located where there is normally a great deal of lightning activity, generally mountain peaks. Since the tower is part of the lightning discharge circuit, the effect of the tower,

itself, on the measurements must be considered. For those measurements reported here, only the raw current measurements are included. Correction for the presence of the tower is omitted because this kind of refinement is not yet available. Also, in mountainous terrain, the behavior of a lightning discharge near the ground's surface is not necessarily the same type of lightning discharge experienced by an aircraft even at low altitudes. Despite the restrictions, tower measurements presently constitute the largest available data base for direct measurement of lightning return stroke currents. Tower measurements have been reported by a number of investigators including the data reported by Uman (Ref. 8), Berger (Ref. 6), and Garbagnati (Refs. 9, 10) discussed in the following literature review.

Unlike Norinder's and Dahle's (see Fig. 8) data collected from remote magnetic field measurements, Uman (Ref. 8) summarizes peak currents primarily measured on towers through various means (Fig. 8). Berger and Vogelsanger, on the other hand, limit their distribution to those strokes with peak currents greater than 10 kA. Their distribution is generally higher than those reported by the other authors and their maximum negative stroke peak current was 105 kA. In his research, however, McCann found a peak value of 160 kA.

By installing magnetic links on transmission line towers, Lewis and Foust (See Fig. 8) collected the largest data set, 2,721 flashes. Their largest measured current was 218 kA, representing the 0.037 percent point in their distribution. A peak current of 120 kA exceeded 99 percent of Lewis' and Foust's measurements. Hagenguth and Anderson, using data measured on the Empire State Building, found a maximum peak current of 58 kA.

Figure 9 (duplicated from Ref. 8) shows data on the rate of rise for lightning discharges to towers. These data based on the current waveforms were also used to produce Figure 8. The rates of rise of the current cannot be derived from the magnetic link data. Importantly since the data presented by Berger and Vogelsanger (Ref. 5) represent the maximum rate of rise in the current waveform, these are typically larger than the data presented by others who used data based on the time the waveform takes to rise from 10 percent to 90 percent of its peak value. While Berger's and Vogelsanger's measurements are more recent than the data from the other researchers, their rate of rise

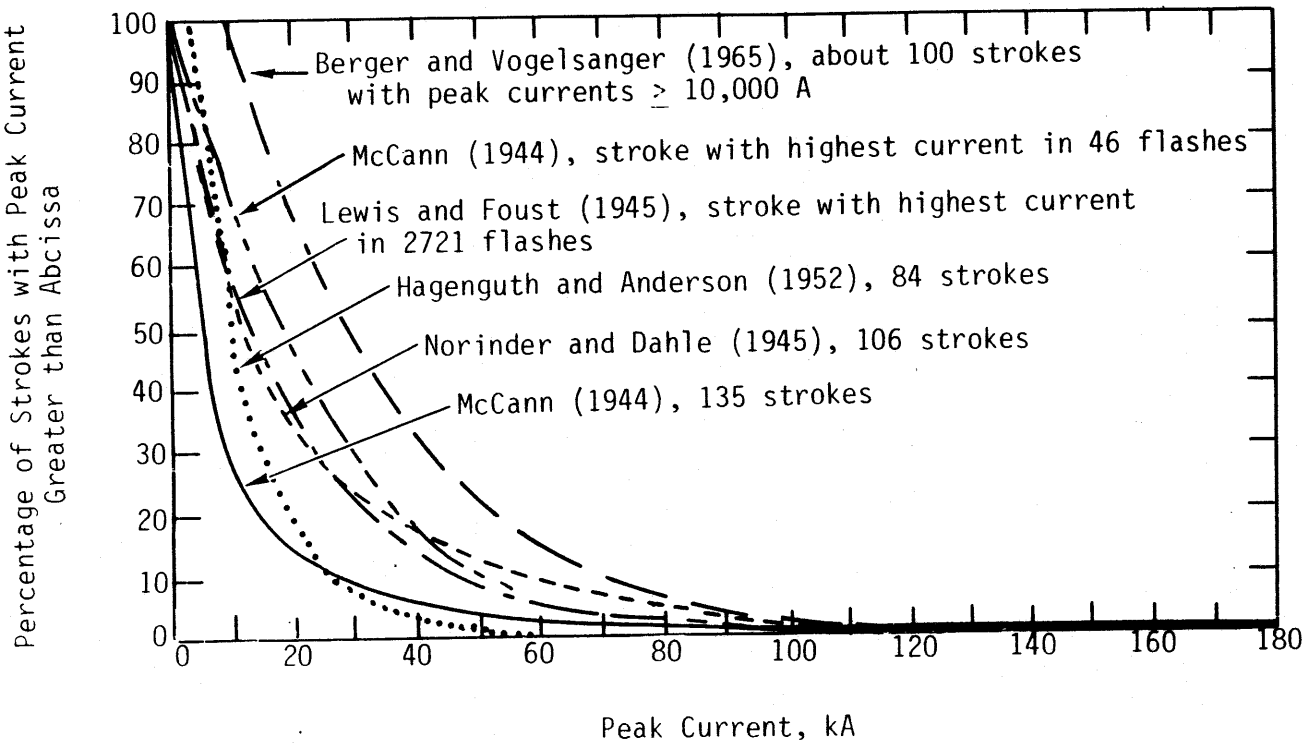

Figure 8. Distribution of peak lightning return stroke currents from various researchers (duplicated from Ref. 8).

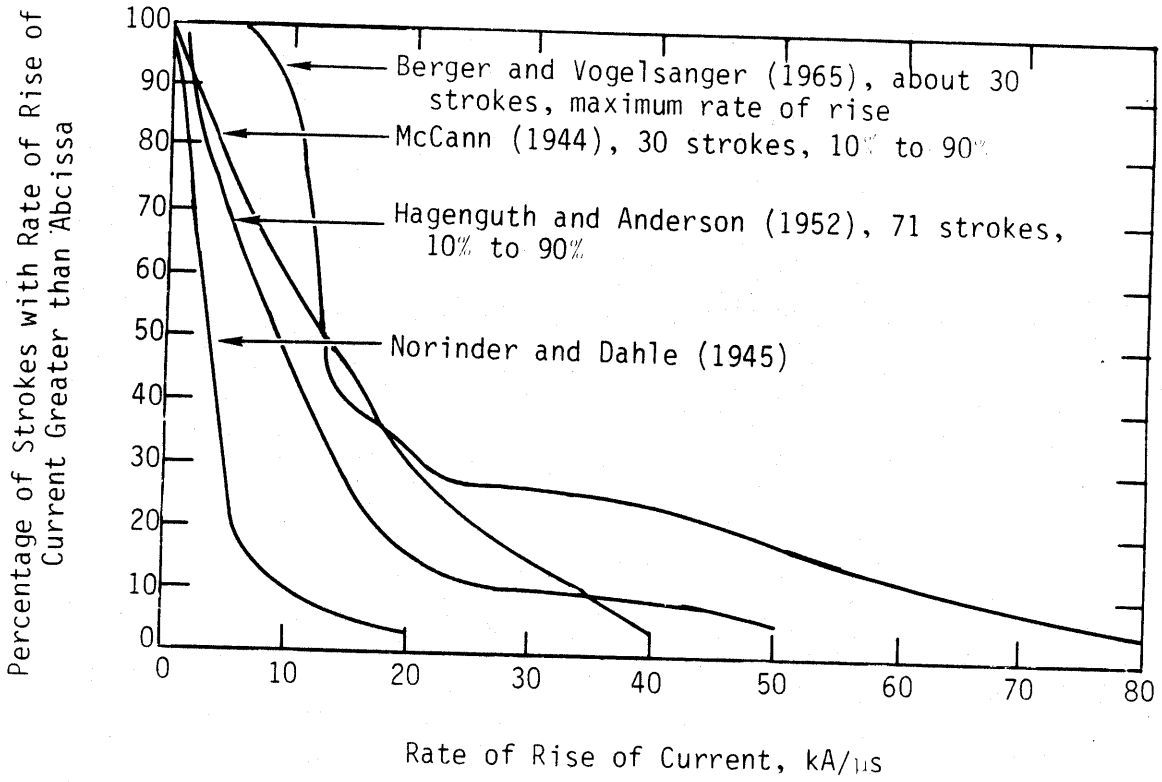

Figure 9. Distribution of observed current rates of rise for various observers (duplicated from Ref. 8).

is calculated differently in that they find the maximum rate of rise of the current and the other researchers use 10 to 90 percent values; consequently, their plot is always larger than the maximum rate of rise given by other researchers.

More recent data showing peak current and maximum rate of rise of the lightning current from tower measurements are presented by Garbagnati (Refs. 9, 10). Figure 10 shows the data for the first and subsequent strokes as well as displaying upward and downward propagating discharges. As this figure demonstrates, the downward traveling currents are larger and the straight line fitted to these data assumes a log normal distribution. The largest of the peak currents presented is slightly above 100 kA.

Data for the maximum rate of rise of lightning current for first strokes and subsequent strokes are shown in Figures 11a and 11b. Again, upward and

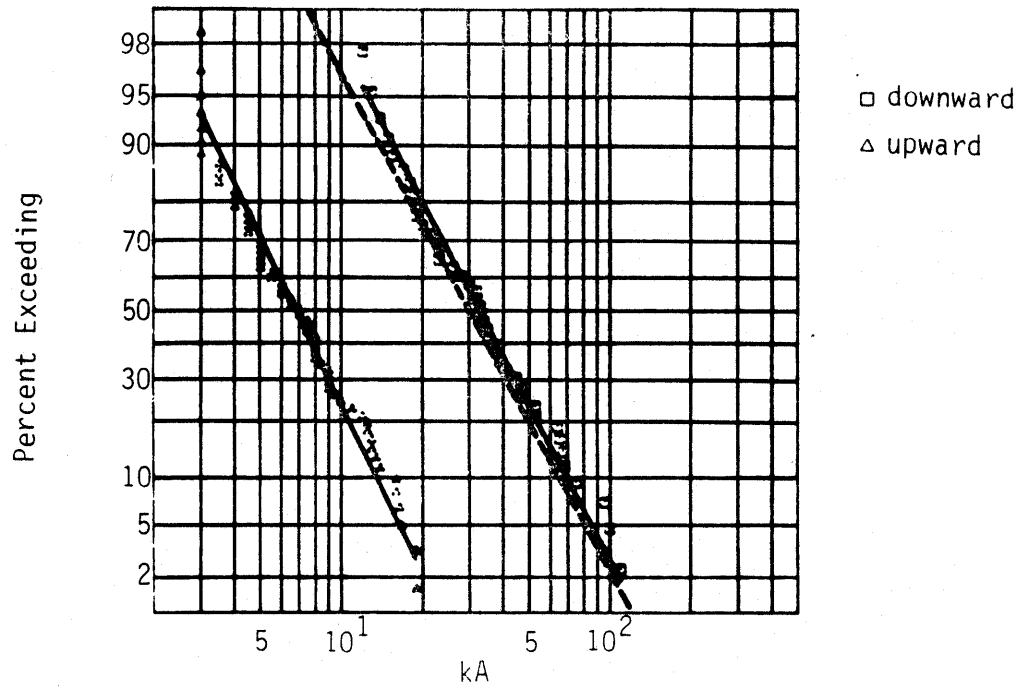

a. First Strokes

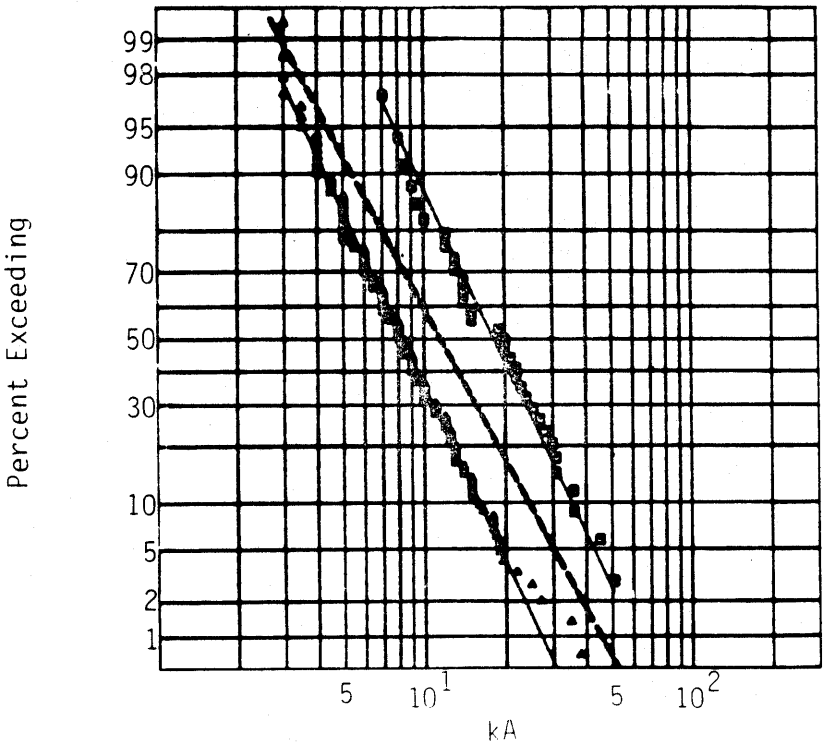

b. Subsequent Strokes

Figure 10. Distribution of peak currents from tower measurements reported in 1982 from Garbagnati (duplicated from Ref. 10).

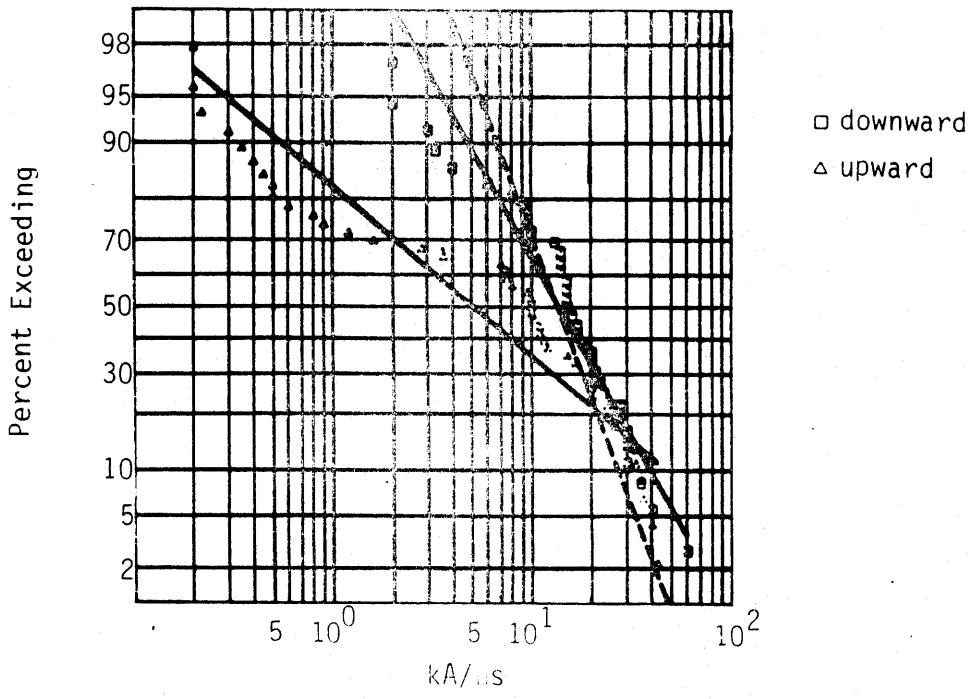

a. First Strokes

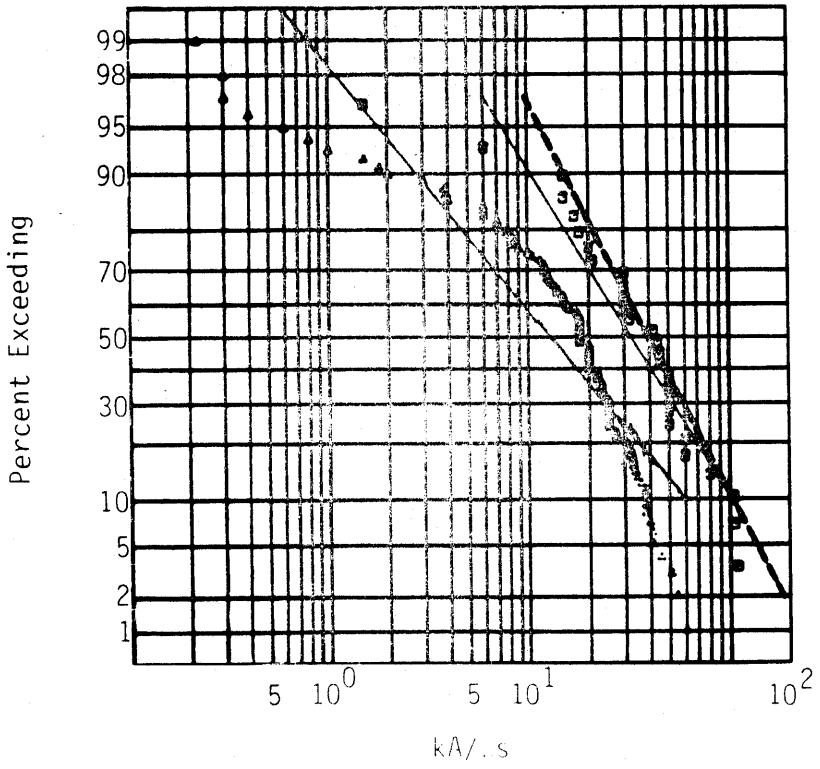

b. Subsequent Strokes

Figure 11. Distribution of current rates of rise for return strokes (duplicated from Ref. 10).

downward strokes display log normal fits. The author, appropriately, only displays the range of the data actually collected; he does not extrapolate. Because graphs should depict only those data actually collected, extrapolating the curve fit beyond the range of data collected is unwarranted. Significantly, extrapolating curve fits to values exceeding the largest data by a factor of three (Ref. 11) is not only not warranted but is scientifically suspect.

Although Garbagnati does not describe his instrumentation in detail in Reference 10 some limits may be deduced by correlating peak current and peak rate of rise data reported in his work (Ref. 10) and reproduced here in Figure 12. A characteristic time for the instrumentation may be calculated by dividing the peak current I_{pk} by the correlated peak rate of rise $\dot{I}_{pk}$. Additionally, the precise minimum time observed by the instrumentation for a particular I, $\dot{I}$ pair indicated by the ratio $I/\dot{I}_{pk}$, where I is the current at the time $\dot{I}_{pk}$ is reached. Since I is not known, an overestimate of $I = I_{pk}$ is used in these calculations. The ratio $I_{pk}/\dot{I}_{pk}$ then represents an upper bound for the minimum time interval measurable by Garbagnati's instrumentation. Lines, showing the ratio $I_{pk}/\dot{I}_{pk}$, have been added to Garbagnati's data in Figure 12. Since there is a data point above the 100 ns line, Garbagnati's instrumentation response time was 100 ns or less. The value 100 ns is also verified in a description of Garbagnati's instrumentation (Ref. 12).

In Figure 13, data from Berger, et al. (Ref. 6) is presented to show a distribution of the maximum rates of rise for different types of lightning currents. Once again, the straight lines represent the assumption of a log normal distribution. Reference 11, however, extrapolates these same data in order to calculate a maximum rate of rise of lightning current at the 1 percent level of the distribution. Such extrapolation beyond the range of collected data, though is unwarranted.

At this time, tower measurements constitute the only low altitude, cloud to ground lightning current measurements available. Although cloud to ground strikes can threaten aircraft in important flight regimes, such as landing patterns and penetration exercises, data for these strikes are hard to obtain. Data to verify or augment tower measurements are difficult to acquire

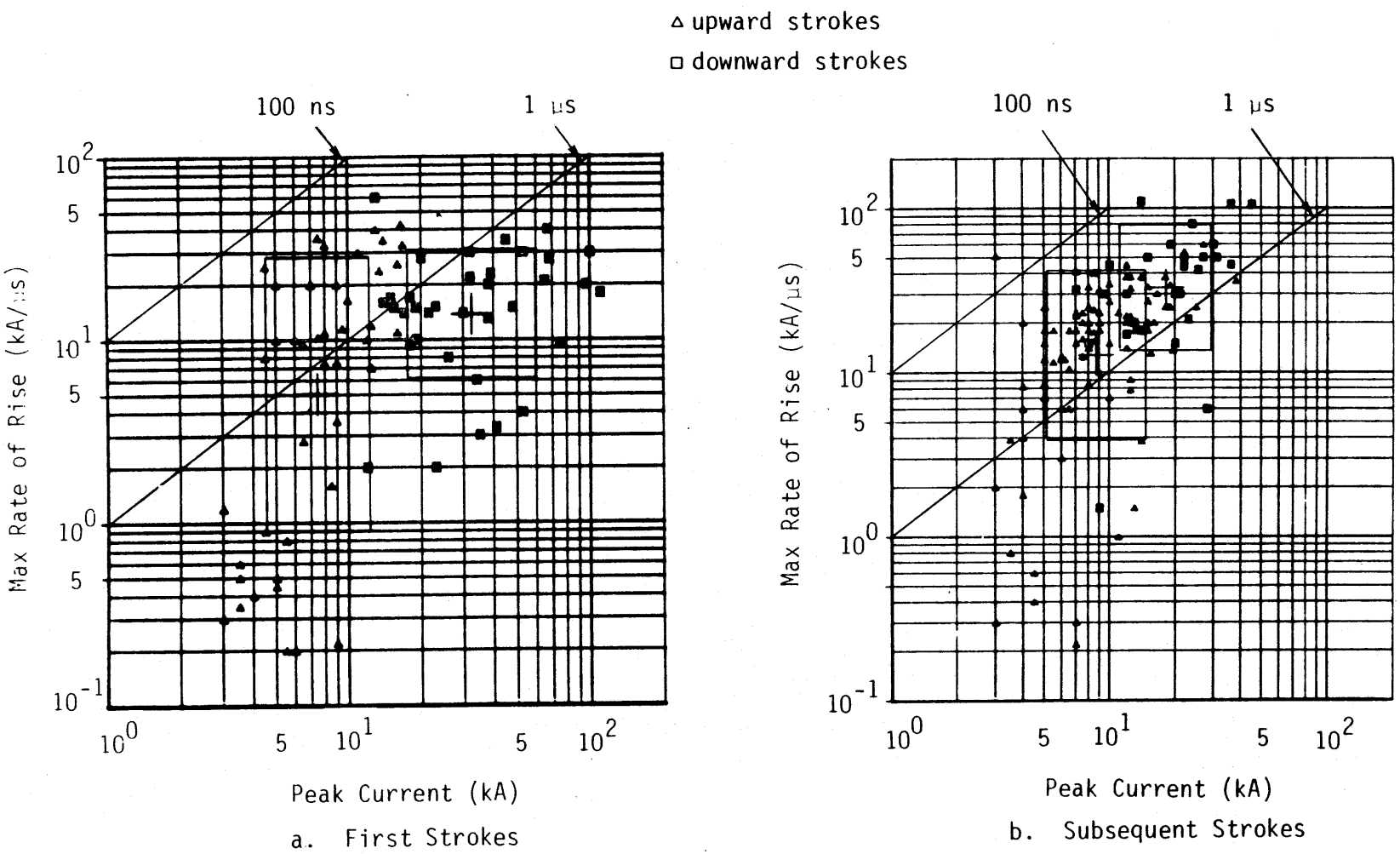

Figure 12. Correlation between current rate of rise and current for first and following strokes--diagonal lines indicate characteristic times, $I/\dot{I}$ (adapted from Ref. 10 by adding lines of characteristic times to the data presented in Ref. 12).

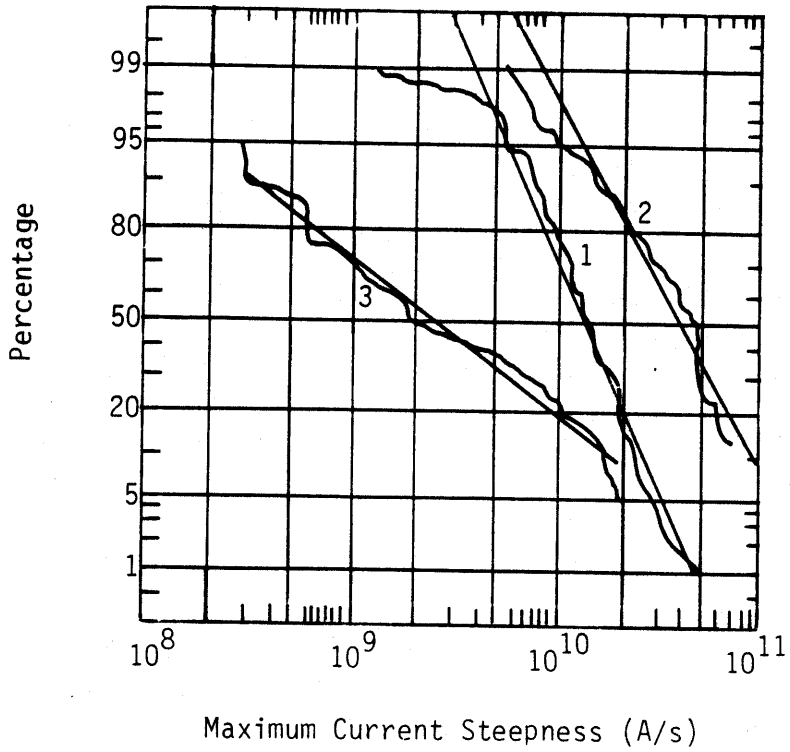

Figure 13. Cumulative frequency distribution of maximum rates of rise of lightning currents. 1. Negative first strokes. 2. Negative subsequent strokes. 3. Positive strokes (duplicated after Ref. 5).

because jet engines operate less efficiently at low altitudes; however, efforts are now underway to improve the data base for these important flight regimes. Even though tower measurements represent the largest data source for cloud to ground strikes, the strikes measured at the towers generally have higher currents than the aircraft measurements (described in the following section). Despite their limitations, tower measurements do provide data on one part of the threat envelope against which aircraft must be protected. Furthermore our concern here is about currents on aircraft moreso than currents in the lightning channel nowhere near a metallic structure; accordingly the tower data are relatively important for our purposes.

Although recent research has increased the data base, several aspects of data collection could be improved. For example, if sufficient analysis could remove the tower's effects from the cloud-lightning-tower-ground circuit, the data would not only improve substantially but would also be more applicable. In addition, quantitatively assessing the instrumentation used in each of the experiments would also be helpful. Although fast response data on cloud to

ground lightning is available from the AFWL sponsored program at Langmuir Laboratory (Ref. 13), it must be fully analyzed before a current waveform specification can be derived.

b. Aircraft Measurements--Electromagnetic measurements made on an aircraft in flight represent another useful data base for determining electromagnetic environment. Since data are generally collected by using fast instrumentation at altitudes above 20,000 feet, they represent the intracloud lightning threat rather than a cloud to ground strike. The data collected from these aircraft measurements, then, help describe high altitude threat to aircraft, just as the tower data help describe the low altitude threat.

Similar to the tower's influence in tower measurements, during aircraft measurements the platform for the measurements, that is, the aircraft, also affects the current. Because of these probable contributory error sources, inferences about the currents on different aircraft must be carefully considered.

Two recent sources provide data on the effects of lightning strikes to aircraft. The first source, a NOAA C-130 aircraft, instrumented primarily to record nearby strikes, recorded two direct strikes (Ref. 14). In these strikes, the maximum rate of rise observed was 3×10^9 A/s for a 3 kA peak current. These results were not limited by the instrumentation bandwidth and were smaller than typical values in the tower samples.

The second source of direct strike data for lightning was an instrumented F-106B operated by the NASA/Langley Research Center during the years 1980 (Ref. 15), 1981 (Refs. 7, 16), 1982 (Ref. 17), and 1983. The instrumentation on this aircraft could record data from sensors up to about 50 MHz and was capable of observing the fast current rates of rise seen on tower measurements. In 1980 and 1981, the $\dot{I}$ measurements were limited by the instrumentation's bandwidth; however, in 1982, with the expansion of the bandwidth faster measurements were available for $\dot{I}$.

The peak rate of rise measured on the boom in front of the aircraft is particularly interesting. In spite of the low (13.9 kA maximum) peak

currents, the peak rate of rise found by taking a graphical derivative of the current records was 1.3×10^{11} A/s. Significantly, the maximum value closely approximates the 10^{11} A/s maximum seen in the tower measurements.

Because the discharges were measured primarily at altitudes above 20,000 ft, the strikes believed to be induced by intracloud discharges, may have been triggered by the presence of the aircraft, itself. Despite efforts to locate cloud-to-ground strikes, however, there have been no successful measurements of cloud-to-ground strikes in the F-106B program. Future efforts in the F-106B program as well as in programs still in the planning stages will be directed toward acquiring data on cloud-to-ground strikes.

For a reasonable worst case flight regime taking place above 20,000 ft, the data supplied by aircraft measurements support using the 10^{11} A/s rate of rise of the current. However, the peak currents observed in these measurements are nearly an order of magnitude lower than the 100 kA reasonable worst case seen in the tower measurements. If a method could be found to separate the effects of the presence of the aircraft from the data, the general applicability of the aircraft measurements would be substantially improved.

c. Currents Inferred from Field Measurements--Another method for determining the current in a discharge is to derive the current from distant field measurements (Refs. 18-21). The difficulty with this method is that the process of unfolding the current in the discharge is complex, nonunique and is affected by the propagation path. While both tower and aircraft measurements require complicated and difficult analysis techniques to remove the effects of either the tower or aircraft from the measurements, the analysis can, in principle, be accomplished. The electromagnetic response of a tower or an aircraft can be calculated to any degree of accuracy the researchers choose to establish. However, in contrast, determining the current in a channel exclusively from the band-limited, noisy, far field measurements of the electromagnetic emission of the channel is a fundamentally more difficult problem.

The most challenging part of the problem is that it is nonunique. Significantly, just because a current may match the measured waveforms exactly does not mean the correct channel current has been found. Recently, researchers

applying a method that uses a particularly simple relation between the currents and radiated fields (Ref. 19) reported a value for the rate of rise of the current of 7×10^{11} A/s (Ref. 22). These figures substantially exceed the values of the peak rate of rise of the lightning current obtained from the data inferred from the tower and aircraft measurements contained in Reference 22.

Since the recent research suggests such a fast behavior for the rate of rise of the current (that is, $\dot{I} = 7 \times 10^{11}$ A/s), in a return stroke the methods used will be more closely examined than the methods discussed earlier.

Uman, et al. (Ref. 19) derive the relationship between the electric field and the current in the lightning channel under a restrictive set of assumptions. For instance, their derivation is based on the current in the return stroke channel propagating up a straight vertical channel without change in the shape of the current waveform. Since the wave is propagating at a constant velocity v, and since it is assumed the fields are measured in the radiation zone of the lightning discharge, the time derivative inside the source integration over the field Green's function may be replaced with a spatial derivative. The source integration, then, becomes trivial (See Ref. 19 for the complete derivation). Under these assumptions, the relationship between the radiated magnetic field and the current waveform is (Ref. 22):

$$\vec{H}_{rad}(D,t) = \frac{v}{2\pi cD}\, i(t - D/c)\, \hat{\phi} \quad , \quad t \geq D/c \tag{3}$$

where

$i(t - D/c)$ is the current waveform in retarded time;

D is the distance from lightning channel to observer;

c is the speed of light;

v is the velocity of propagation of the current pulse;

$\hat{\phi}$ is the unit vector in the ϕ direction of a spherical coordinate system centered at the base of the lightning channel.

The assumption that a current waveform propagates undisturbed along the channel at a constant velocity is equivalent to treating the return stroke

discharge as a lossless transmission line for the early part of the discharge. In their work for example, Master, et al. (Ref. 21) present a postulated breakdown current waveform that also contains a factor of $e^{-z/\lambda}$, where λ = 1500 m to account for the observed decrease in channel brightness with height (Ref. 23). This variation with height, however, is not consistent with the lossless transmission line assumptions of Reference 20 from which the current waveform parameters were derived. These parameters are shown in Equation 3 of this paper and Equation 8 of Reference 19. The variation of height is also not consistent with a resistive transmission line.

As the authors note (Ref. 20) the current obtained from the radiated fields using any method is not unique. Consequently, the conclusions about the current in a lightning discharge made from field measurements can be refuted merely by determining that an alternate model is consistent with the physics of the problem. However, when anomalously large values for $\dot{I}(t)$ occur (Ref. 22), a search for other possible models is clearly appropriate.

One possible model is based on the diagrams in Figure 14. Assume the downwardly moving lightning channel initially attaches to an upward streamer at a height D, the so-called striking distance, typically of the order of $\approx$100 m. Before attachment, the voltage, V, on the channel can be represented as two oppositely directed waves of voltage, V/2 (Fig. 14a). They carry opposite currents which sum to zero net current. The downwardly propagating wave, then, is reflected by the open (infinite resistance) termination into the upward wave.

Upon attachment, however, this reflection changes. For instance if the characteristic impedances of the channel above and below are the same, there is no longer any reflection. At a time t after attachment (Fig. 14b), we have at distance ct below D a downward wave of current i = V/2Z, where Z is the characteristic impedance. Above D we have at distance ct an upward wave of the same current. Thus, because the currents are both directed upward we have a monopole source. It should be noted that although a current monitor near the base of the channel (that is, a Rogowski coil on a tower struck by lightning) would measure this i, the radiated fields would be double those inferred

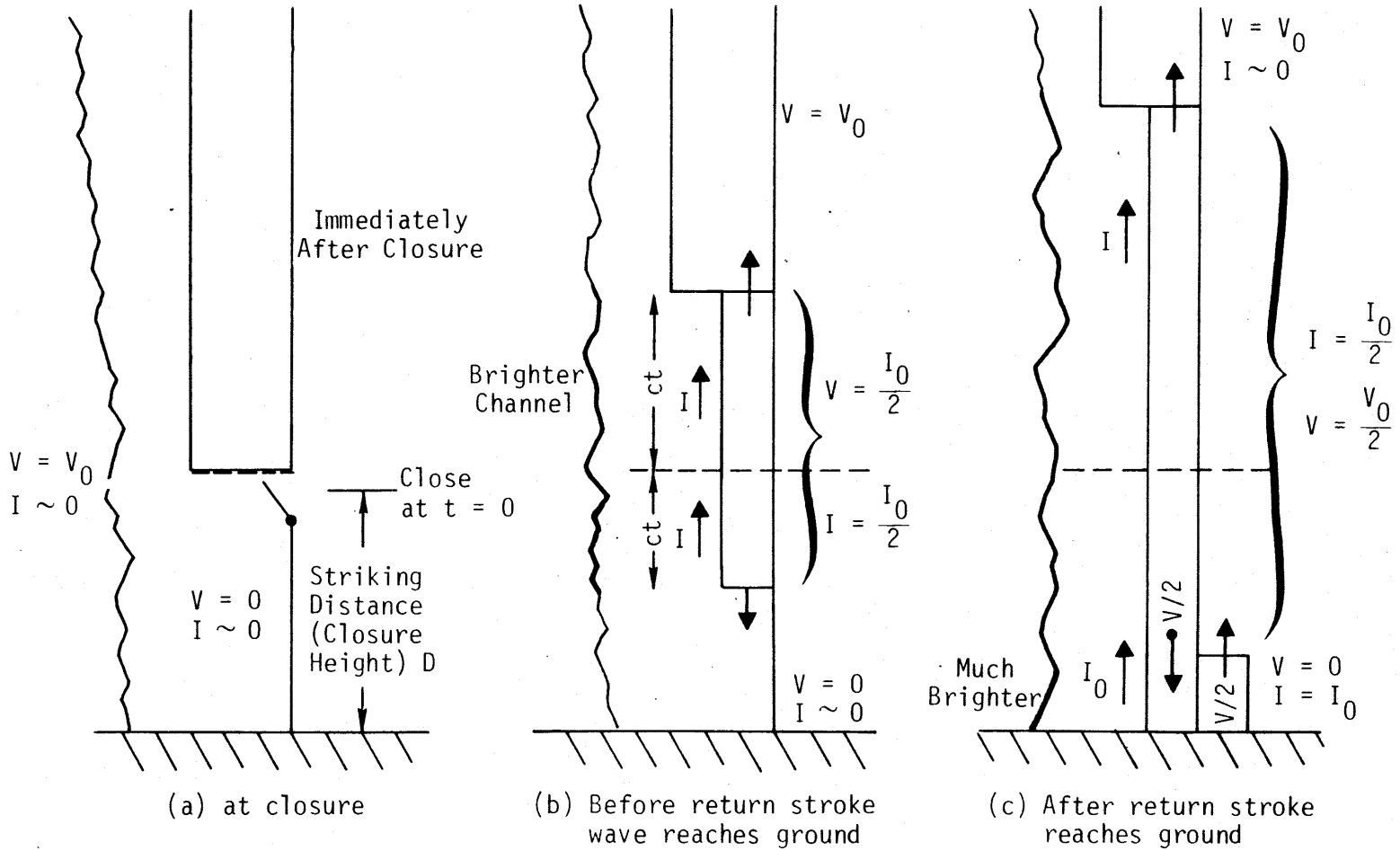

Figure 14. Hypothetical sequence of waves on a lightning channel following closure of upgoing and downgoing leaders.

when the current along the striking distance of the channel, due to the contribution of the upwardly propagating wave, is assumed. This doubling is in addition to the usual doubling of radiated fields by the ground plane.

At time t = D/c (c is the wave speed), the downward wave reaches the ground. If this impedance is low, then a wave of voltage -V/2 is reflected, resulting in the lowest portions of the line being at ground potential. Subsequently, two current waves propagate up the channel, the lower carrying I = V/Z and the upper one-half that.

The concept of a downward going leader converging with an upward going leader are initiating a return stroke has been described by Uman (Ref. 24) and by Berger (Ref. 25) with a striking distance D (where the two leaders converge) about 100 m reported by both researchers.

Such a model, however, is inappropriate for subsequent strokes because the dart leader descends smoothly along the previous return stroke channel and initiates a subsequent stroke at ground level. A physical description based on the mechanics of streamer propagation and subsequent return stroke behavior near the ground may be considered. A dart leader channel behaves as a charged, moving cylindrical conductor near a ground plane. As the current pulse nears the ground plane, fields along the previous return stroke channel exceed breakdown. Although the breakdown field value is not known, its value is most likely lower than that for undisturbed air. Information about the field exceeding the breakdown level suggests that it travels at the velocity of light, rather than the smaller velocities of breakdown waves. Apparently, near earth, the early behavior of subsequent return strokes may be governed by the velocity of light rather than the characteristic of v = c/3 usually associated with return strokes. Furthermore, velocities are known to be higher in subsequent strokes (Ref. 26).

The effects of the additional factor of two in the relationship between signal and channel current as well as an increased velocity of the return stroke near the initiation region can be compared to the simple transmission-line model. Such a comparison may be seen from a reproduction and subsequent adaptations shown in Figures 15a-15d, adapted from Reference 27.

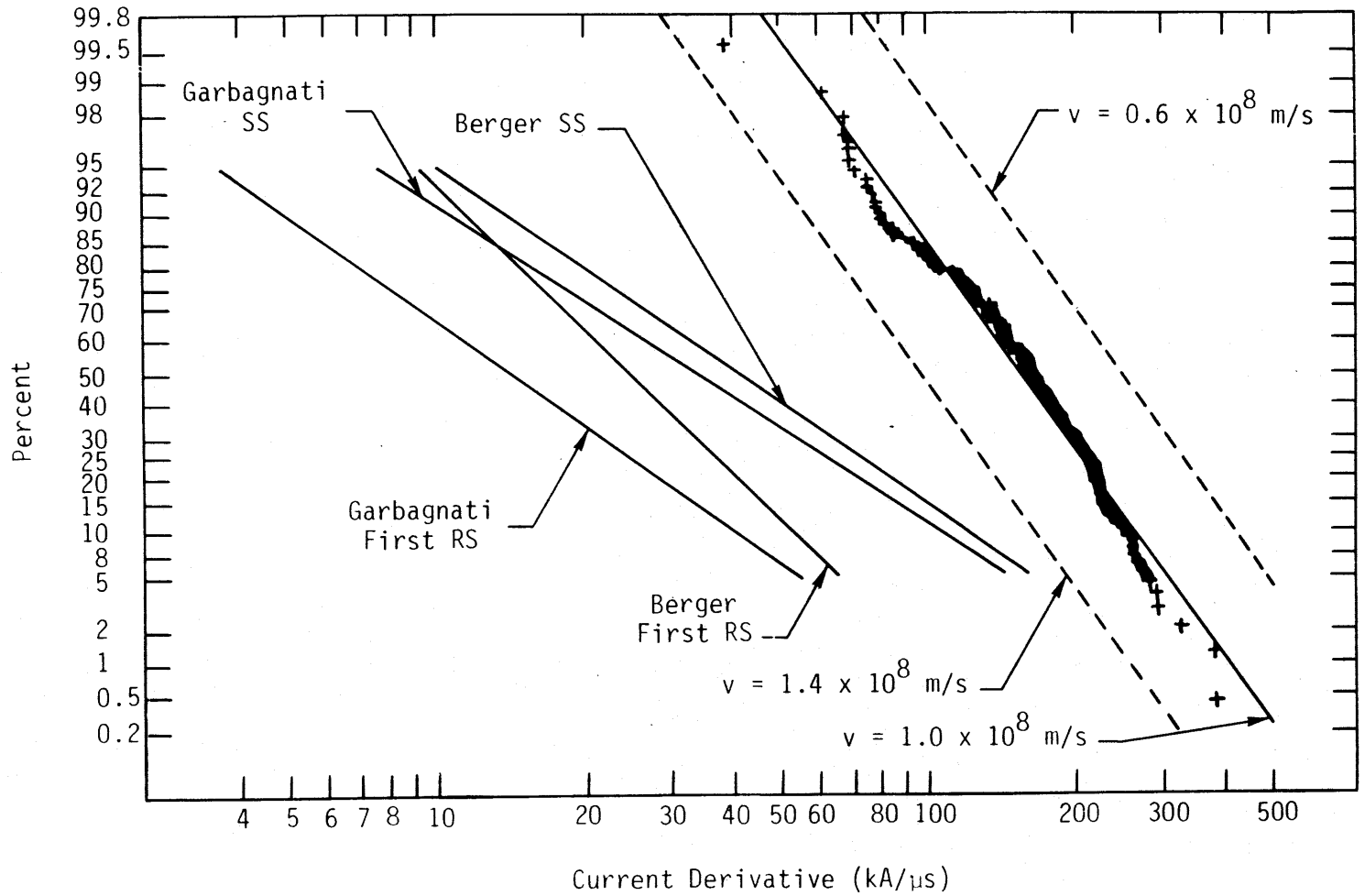

Figure 15a. Data on the distribution of lightning currents as derived by Krider and Weidman (Ref. 27) compared to distributions published by Berger and Garbagnati.

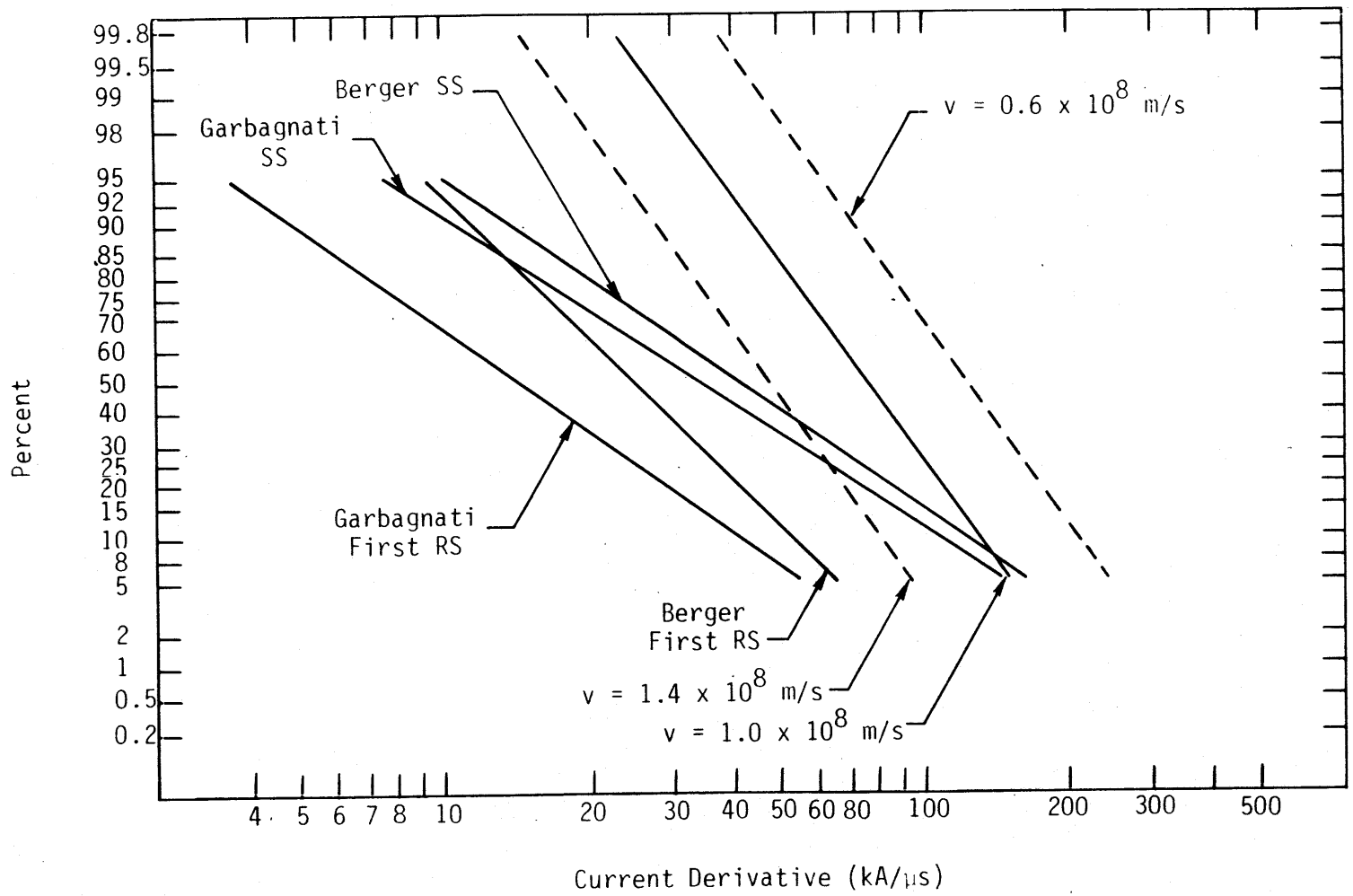

Figure 15b. Same as Figure 15a except that the distribution of Krider and Weidman is corrected for the factor of two in the initiation phase for first strokes.

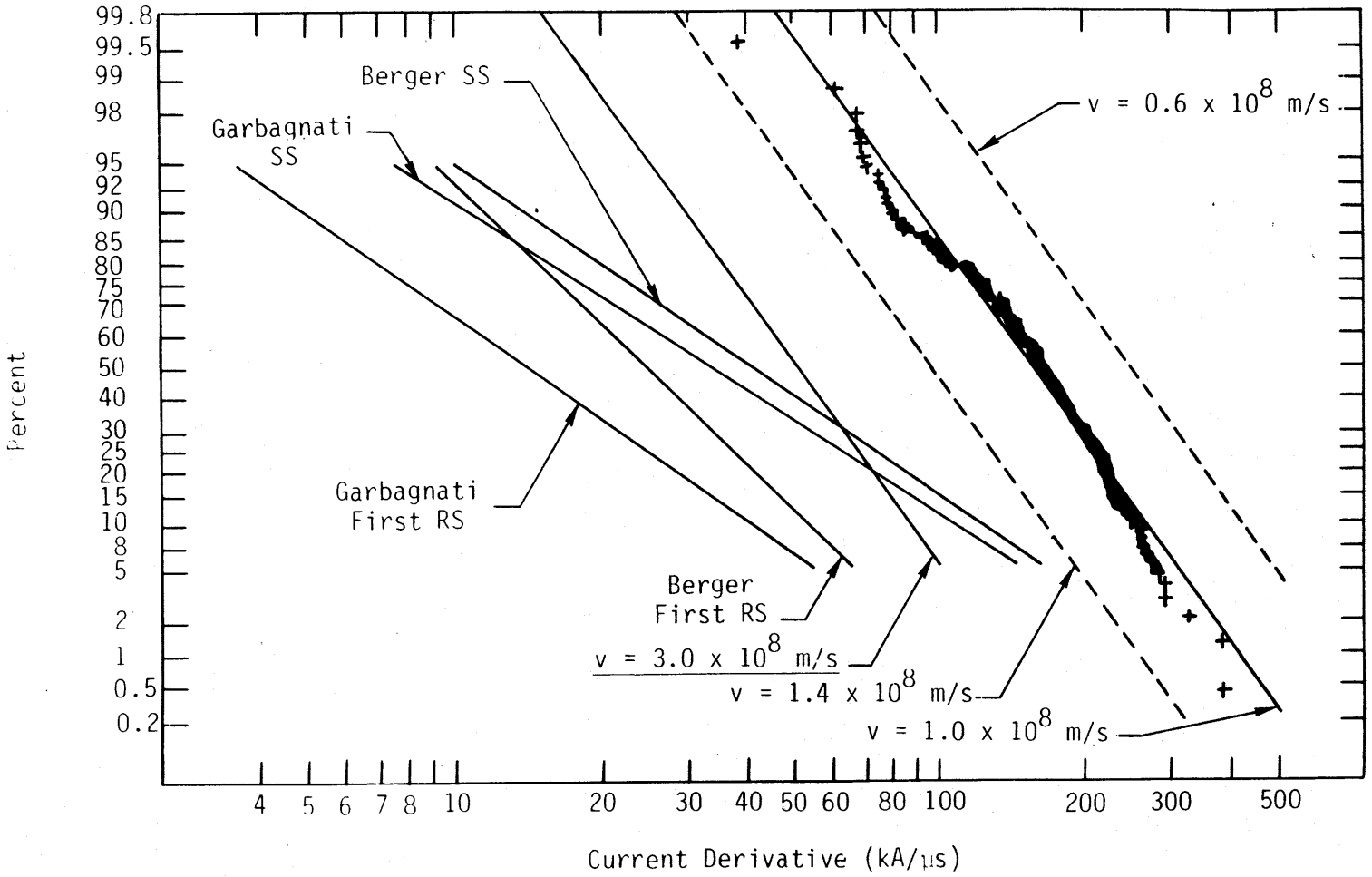

Figure 15c. Data of Figure 15a with the addition of a line which shows the effect of a fast velocity near the ground where fields are large. The underlined caption indicates the added line (adapted from Ref. 27).

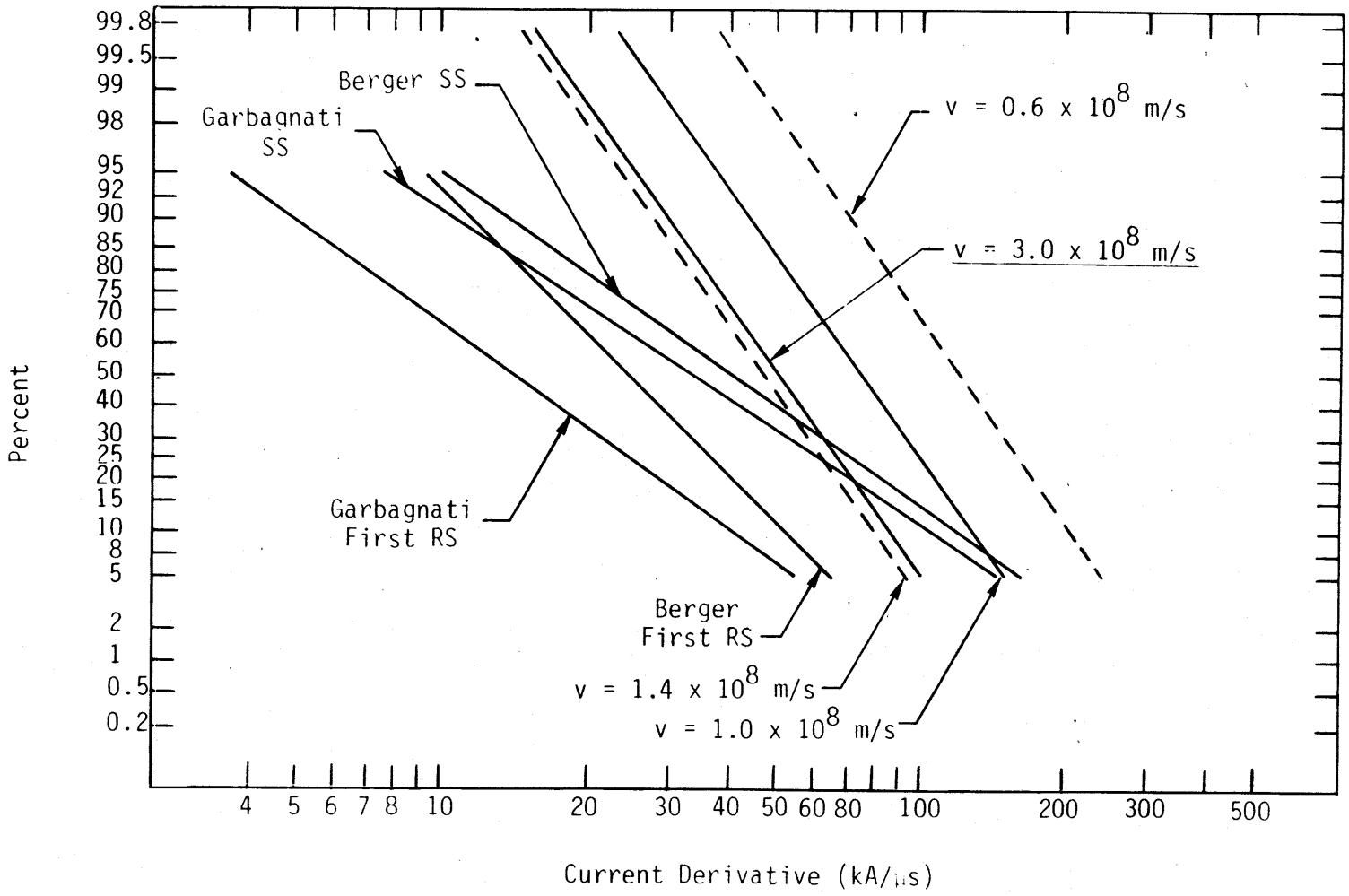

Figure 15d. Data of Figure 15b with the addition of a line which shows the effect of a fast velocity near the ground where fields are large. Note the close agreement at the high current levels.

These differences may be seen by comparing Figure 15a with two adaptations. (Fig. 15a is a reproduction of Fig. 7 from Ref. 27. The three adaptations are numbered 15b, 15c, and 15d, respectively.) Figure 15b, modified from Figure 15a, accounts for the factor of two for the first strokes. Figure 15c, another modification of Figure 15a, accounts for an upper limit of a characteristic velocity of c in the initiation region. As these two figures (15b, 15c) clearly show, these corrections substantially improve the agreement of the data, shown in the original figure (15a), with the data provided by Garbagnati (Ref. 10) and Berger (Ref. 6). Figure 15d combines the changes of Figures 15b and 15c for clarity.

Further consideration of the initiation region (Fig. 14) suggests that perhaps a lossy transmission line model would more adequately describe the region than the lossless transmission line model used to derive Equation 3. Resistivity per unit length of the channel is calculated easily from derived air conductivity values (Ref. 28).

During the initial stage, the return channel radius is small; consequently the channel is simultaneously resistive and inductive (Refs. 28, 29). More recent detailed numerical studies show that the channel diameter is also quite small, limited only by the mean free path for collisions in the channel. For the diameter of the return stroke, an initial value of 2 mm is both consistent with these last three references and with Uman's measurements (Ref. 30). However after several microseconds, the channel grows larger; as the channel area increases, the resistivity decreases.

Although the plasma in the return stroke channel is conductive, its conductivity depends on the temperature and density of the channel. The value ($\sigma = 2.2 \times 10^4$ S/m) for a hot channel is reached only in the later stages of the channel's development. This high value of the conductivity, by initially forming an upper bound on the channel conductivity at early times, allows simple calculations. A plot of the values of conductivity of hot equilibrium air for various pressures is shown in Figure 16 (Ref. 31). For highly ionized air, the electrical conductivity tends to decrease as the temperature increases. This occurs because collisions of the conducting electrons with

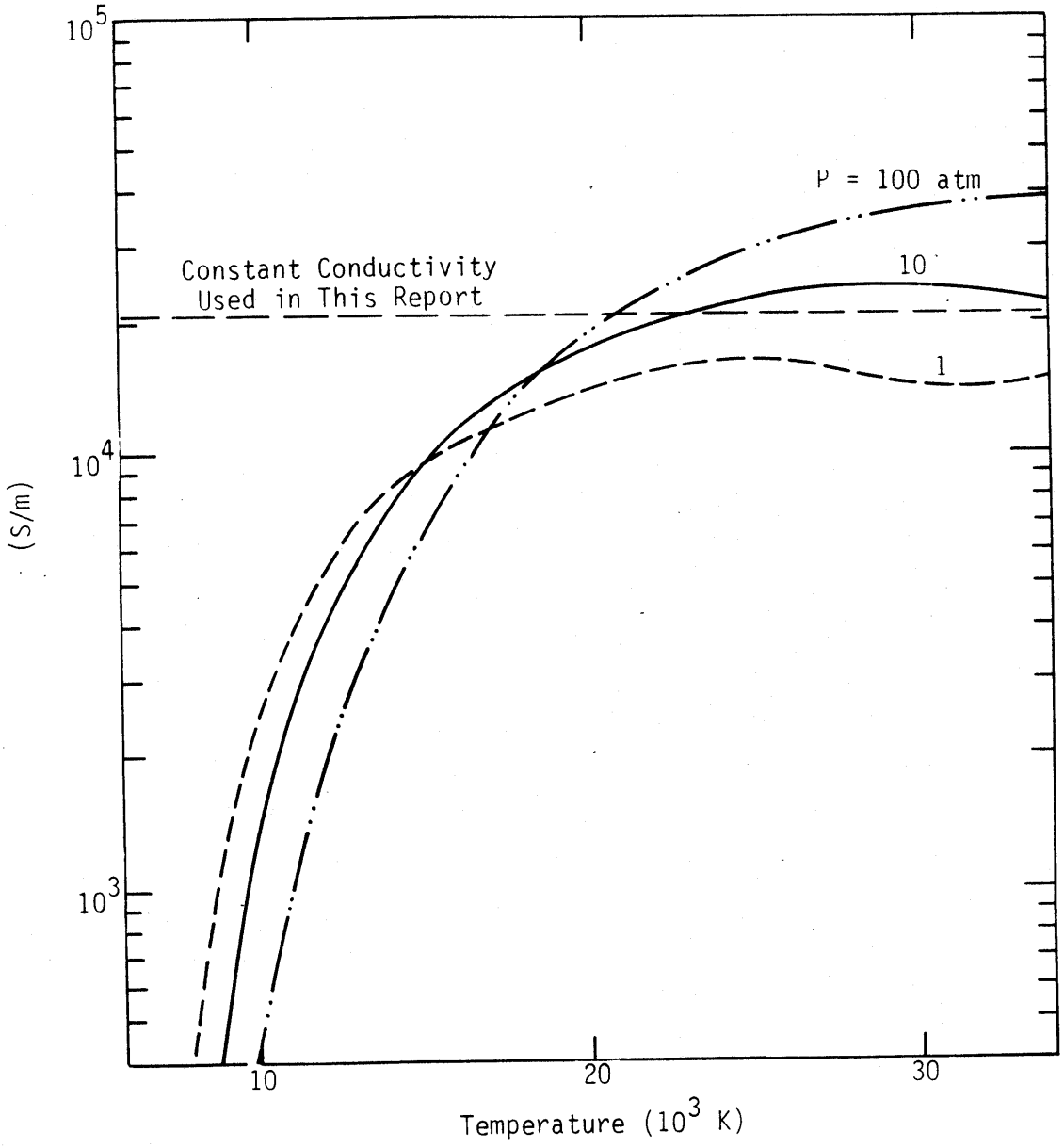

Figure 16. Electrical conductivity of an air plasma, at 1, 10, and 100 atm pressure, versus temperature (adapted from Ref. 31).

ions dominate the effect of collisions with neutrals as the source of resistivity. Since this type of plot for the conductivity of air is good for all hot air regardless of the cause of the heating, it is good for lightning. Estimates of the peak internal temperature of lightning are available from spectroscopic measurements (Ref. 31) and are below the 30 kK shown in Figure 16.

The resistance of a 1 m length of channel then may be calculated. Using the above channel radius (a = 1 mm) and electrical conductivity ($\sigma = 2.2 \times 10^4$ S/m), and assuming a cylindrical channel allows calculation of the resistance per unit length of the channel, R'.

$$R' = \frac{1}{\pi a^2 \sigma} = 14\ \Omega/m \tag{4}$$

For a low-loss transmission line, the current is attenuated as $e^{-\alpha z}$ (Ref. 32) where:

$$\alpha = \frac{R'}{2Z_0} = 0.02\ m^{-1} \tag{5}$$

and where Z_0 is the characteristic impedance of the line about 300 Ω (Ref. 33). The e-folding distance (distance to 1/e or 37 percent of original peak value) is then only about 50 m, for the leading edge of the current. As the channel expands, of course, the resistivity decreases reaching a value equivalent to an e-folding distance of 5 km after about 10 μs, and then the rate of expansion slows substantially. Since the e-folding distance is only about 50 m, high frequency components of the discharge are localized. This is in contrast with the high frequency components that propagate undistorted for 100 m or more. This kind of propagation is required by the assumptions used to support the model of the relation between the fields and current (Ref. 19; Eq. 13).

A physical picture of the early time behavior of the return stroke from a cloud to ground discharge would depict a charged leader channel from the cloud meeting a channel growing up from the ground. When the two meet, the upper

channel begins to discharge into the lower channel. The volume where the channels meet can be called the initiation region. The result is two current waves traveling in opposite directions from the point of intersection (in a transmission line analogue sense, the point of switch closure). Both current waveforms radiate, as in Figure 14, demonstrating the factor of two difference in the results (Refs. 20, 22, 27). Researchers have typically treated only the upgoing wave for a first stroke as noted in a discussion earlier in this section.

If the high frequency fields are generated primarily in this initiation region as demanded by the arguments associated with Equation 5, rather than over a long transmission line segment, then the relationship between the current and the radiated fields differ significantly from the relationship suggested by Equation 3. For a local dipole model of the initiation region,the radiated fields are given by (Ref. 34):

$$\vec{H}_{rad} = \frac{\ell}{2\pi Dc} \frac{\partial I(t)}{\partial t} \hat{\phi} \qquad (6)$$

where ℓ = characteristic size of the initiation region, and the other variables are consistent with the definitions in Equation 3.

Since the radiated fields for this model are proportional to $\partial I/\partial t$ rather than $I(t)$, the integral of the field is appropriate to use for the current waveforms rather than the field waveform. This argument implies more slowly rising currents than the results contained in Uman, et al. (Ref. 22).

d. Effect of branching--There is another mechanism that may account for the fast behavior of the fields measured in the far field of a lightning discharge. The data examined appears in Figure 3 of Reference 35 and is reproduced in our Figure 17. Electric field is plotted relative to the corresponding rate of rise of the electric field. The data appears in two clumps, with about 20 percent of the data appearing with both significantly larger electric field and rate of rise of the electric field than the centroid of the smaller clump. It seems possible that at least the high level clump the two clumps

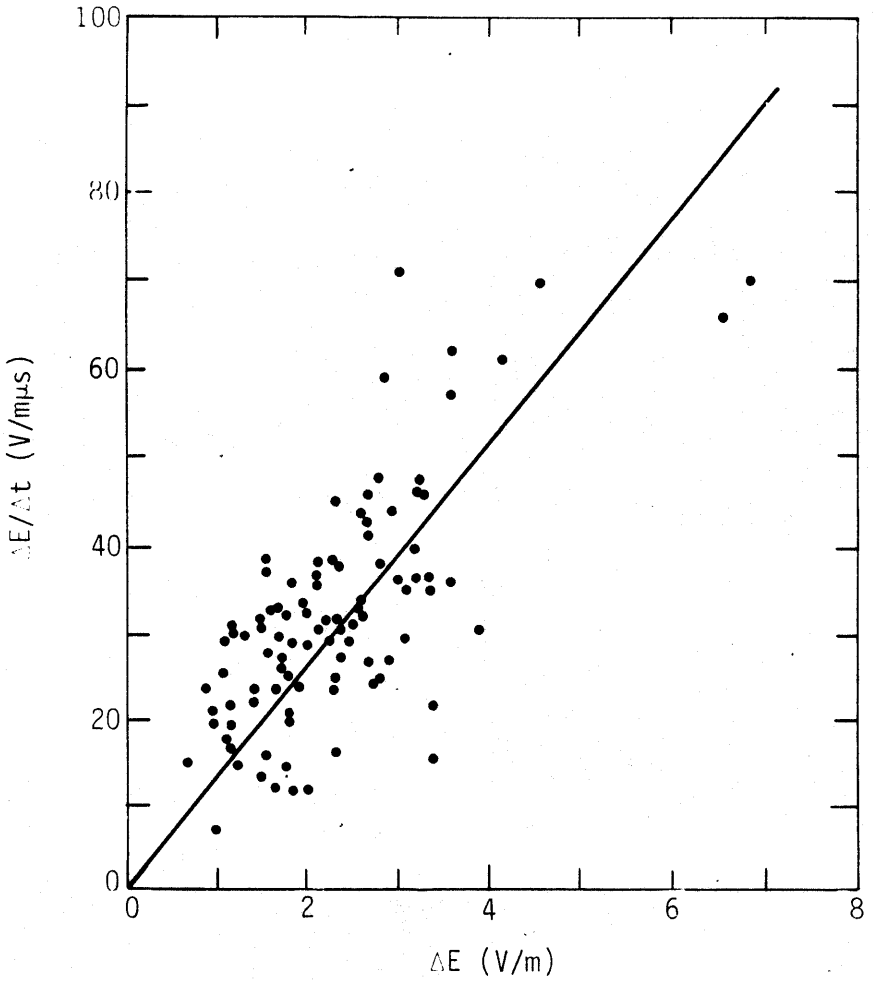

Figure 17. A histogram of the maximum rate of rise of the fast transition in return stroke E fields from range-normalized to 100 km. Reproduced from Reference 1.

and some of the spread of the data is due to branching of the channel near the ground. An example of a branched leader is shown in Reference 36 with photographs from a television camera for two different times are reproduced in Figure 18 of this paper. Note that the whole sky camera is located 45 m North, 16 m East and 6 m above Kiva 1 which is the center of coordinates for Figure 19. In Figure 19, there is a superposition shown of acoustic transducer location and an estimate of the positions of the electromagnetic sources showing the three branches. The branches are not quite simultaneous.

The mechanism by which increased electric fields and corresponding rates of rise are produced at early times is shown in Figure 20 with the overall scale of the problem taken from the data of Reference 36. The following assumptions are used in the attempt to understand the behavior of branched return strokes.

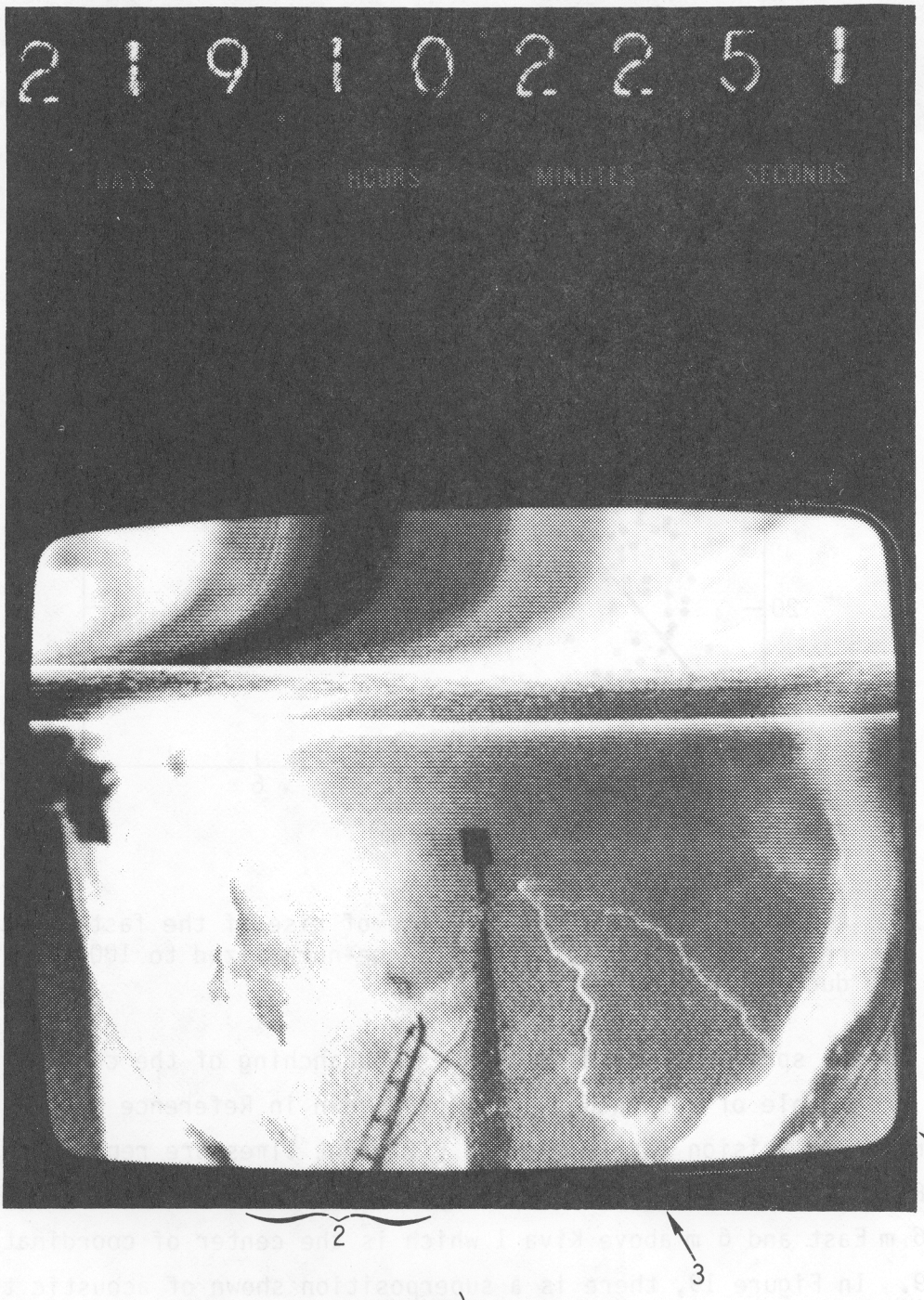

a)

Figure 18. All sky photographs of a three-branch discharge at two different times (Ref. 36).

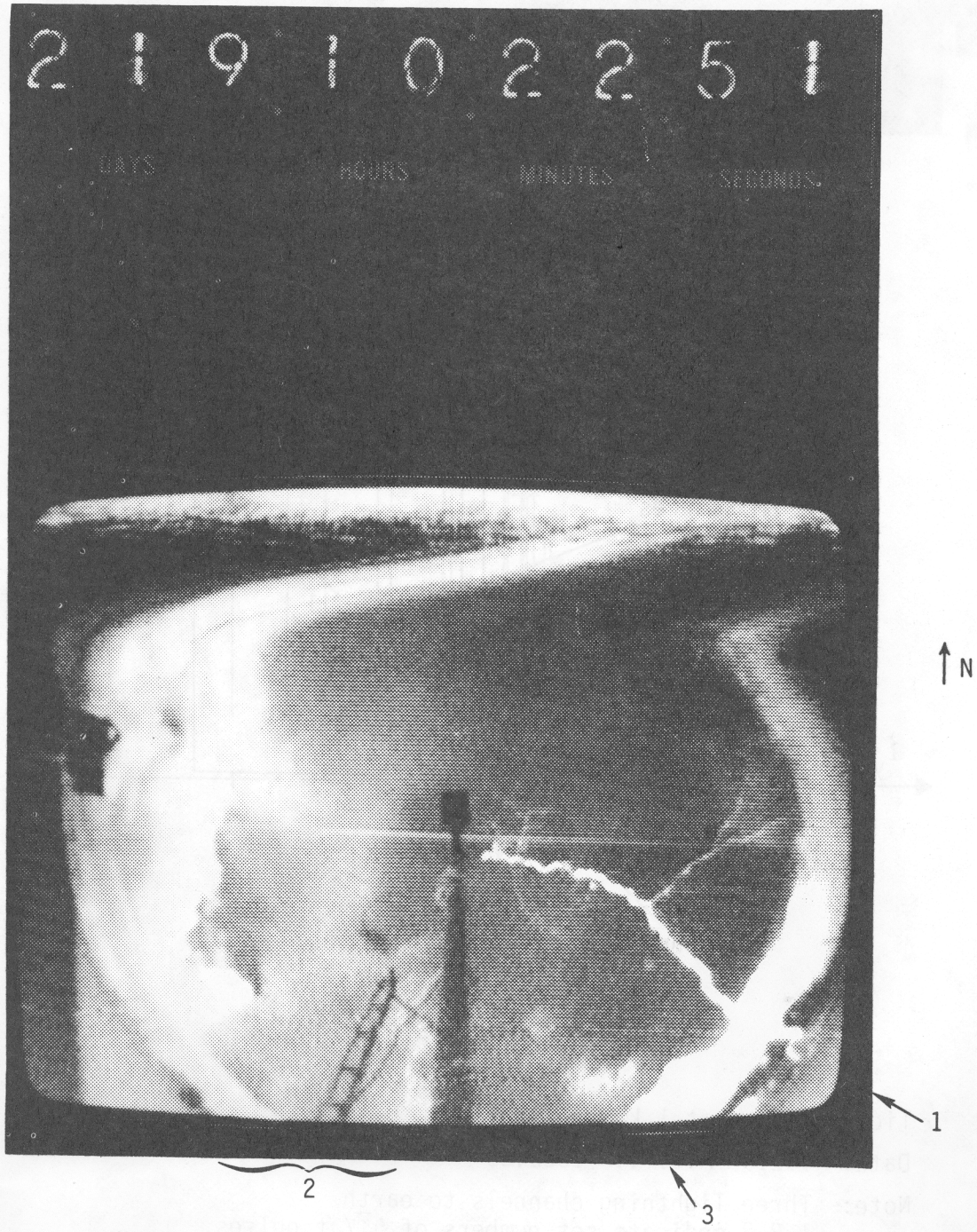

b)

Figure 18. Concluded.

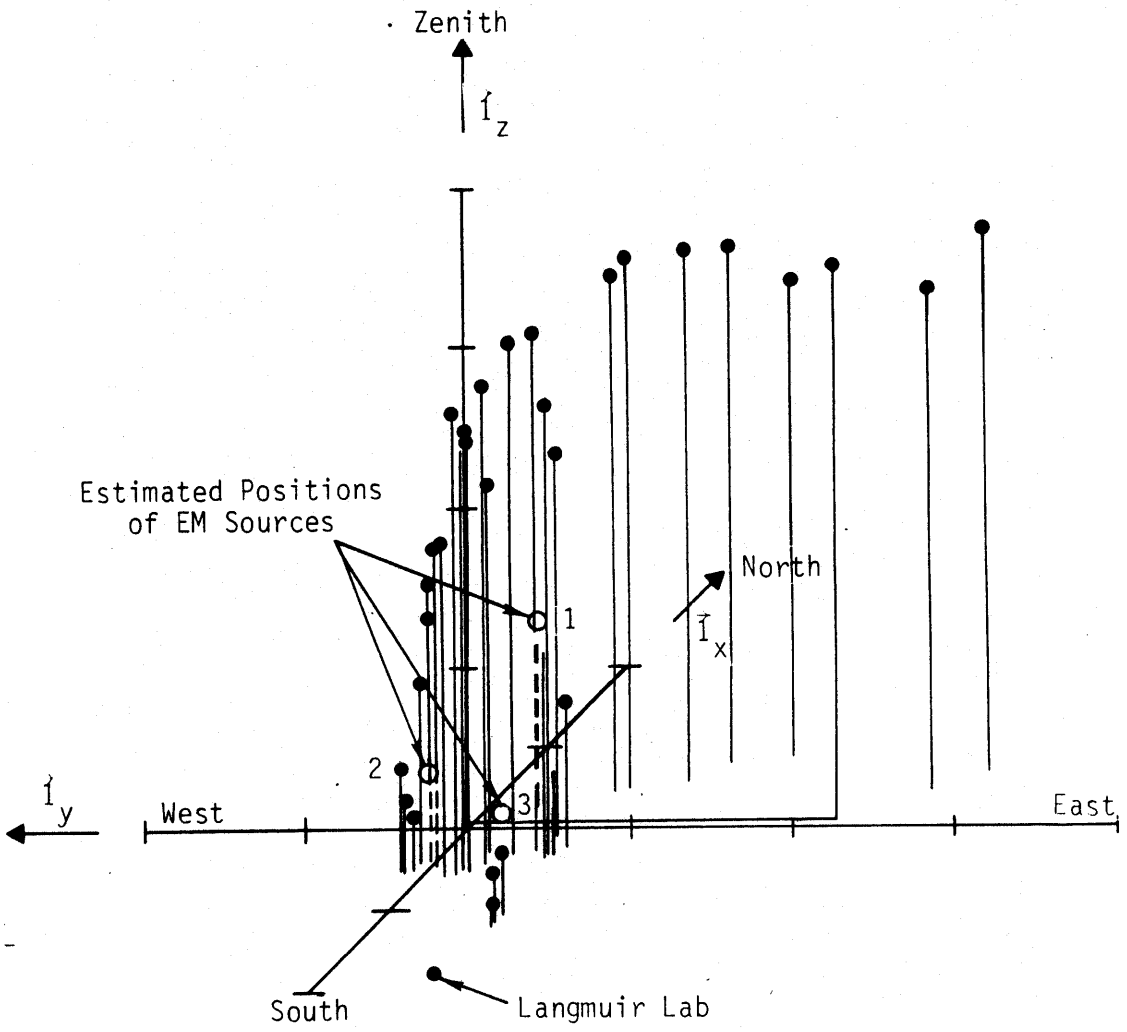

Ticks on axes at 1 km intervals.

Date: 79219 M.S.T.: 1022:51

Note: Three lightning channels to earth
1,2,3 indicate set numbers of $\delta\vec{T}/\delta t$ pulses.

Figure 19. Acoustic location of midrange leader(s) (Ref. 36).

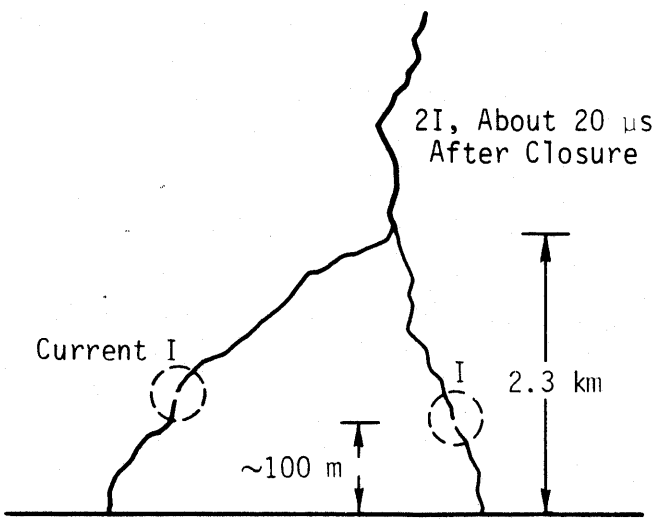

Figure 20. Possible branched configuration showing closure region where the transition from leader to return stroke occurs.

(a) There is a region of switch closure as discussed earlier for the single channel leader-return stroke transition.

(b) The high frequency components of the current are determined exclusively by the local behavior of the closure region, specifically including the magnitude of that current.

(c) The voltages at the closure points, the altitude of the closure locations, and the time of closure are roughly the same for each branch and independent of the number of branches.

Under these assumptions, both the electric field and rate of change of the electric field are increased by the number of channels. For the three branch system shown in the photograph (Fig. 18) each of the parameters is increased by addition of the parameters from all branches, giving at most a factor of 3 increase over the largest. The uppermost data points in Figure 17 correspond to such a configuration.

The conclusion one should draw from such a model of the branched structure is that the maximum fields and rates of rise of the fields are not the values that are indicative of the most hostile conditions local to the strike,

particularly in the closure region which produces most of the high frequency content.

However, this discussion of models of the electromagnetic fields produced by lightning channels clearly demonstrates that the generation of high frequency fields by lightning channels should not be limited to the very simple model represented by Equation 3. Since the initiation region of a return stroke is an extremely complicated and poorly understood part of the lightning discharge process, a very complicated model must be used to provide a quantitative physical description of the initiation region. This model, however, must be secure in the inverse processes used to determine the lightning current from distant fields, particularly from noisy measurements.

Even though alternative physical descriptions of the lightning channel exist and even though these may differ from the parameters assumed in Equation 3 and presented in other research (Refs. 19-22), such physical description should also be used cautiously. Specifically, the values of the parameters, like the peak rate of rise of the return stroke current that was derived by applying inverse processes to Equation 3 should not be assumed to be very accurate. The assumption of accuracy is particularly inappropriate when the results of those calculations diverge from other experimental results.

3. SUMMARY OF THE LIGHTNING THREAT

A review of the available data suggests that at least one waveform is a severe threat for the lightning return stroke current. This simple waveform which has an analytic Laplace transform and proper behavior of its derivatives at its initiation point is a modification of the waveform described by Equation 2. Although this equation is nonzero at all negative times, the offset time, t_0, may be selected to make the error associated with currents at negative times as small as desired. The lightning current may be described by:

$$I(t) = \frac{kI_{pk}}{e^{-(t-t_0)/\tau_r} + e^{(t-t_0)/\tau_f}} \qquad (7)$$

where

k is 1.025 and I_{pk} = 100 kA

τ_r is the rise time constant = 2.5×10^{-7}, chosen to give a maximum rate of rise 10^{11} A/s at $t = t_0$

τ_f = 50 μs is the fall time constant

t_0 is an offset time

Figure 21 is a plot of the current described by Equation 7 and Figure 22 shows its derivative. Note the smooth behavior of the derivatives throughout its range. Figure 23 shows the corresponding frequency spectrum for the waveform described by Equation 7. Based on an examination of the tower data, aircraft data, and inferences from field measurements, the peak current, I_{pk}, for the reasonable worst case waveform is chosen to be 100 kA. The 100 kA value corresponds to the 2 percent level of the distribution, and to the maximum value reported by Garbagnati (Ref. 10). Values for peak currents above 100 kA have been rare for other researchers who have reported tower measurements of return stroke currents. The early time characteristics for this waveform are chosen to correspond to a maximum rate of rise of 10^{11} A/s for the return stroke current. The value of 10^{11} A/s corresponds to the largest value of $\dot{I}(t)$ reported by Berger or Garbagnati and is also very close to the maximum value (1.3×10^{11} A/s) seen by the 1982 F-106B program (176 strikes). Credibility of the larger values derived from field measurements suffers from a lack of data or theory describing the distribution of the current waveform as a function of position along the return stroke channel. The characteristics of lightning return stroke currents that occur on long timescales are well known and the figure of 50 μs for the duration of a single return stroke current pulse reported by Cianos and Pierce (Ref. 37) and Uman (Ref. 5) is not disputed in this report.

A moderate threat may also be defined. A value of 10 kA for the peak current is consistent with the maximum value of 13 kA seen on the F-106B aircraft program in 1980-82. The rate of rise of the current pulse seems more characteristic of the discharge process than of the peak current (Refs. 38-39), so the maximum rate of rise should remain at $\dot{I} = 10^{11}$ A/s for the moderate threat as well.

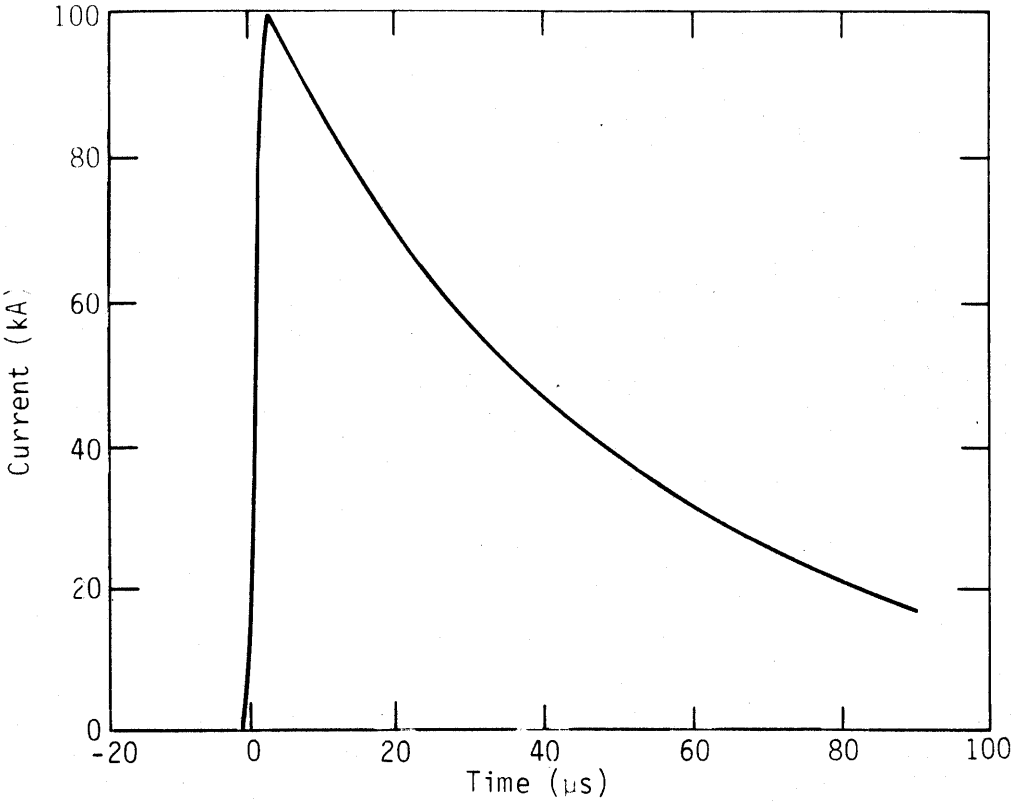

Figure 21. Waveform of current described by Equation 7.

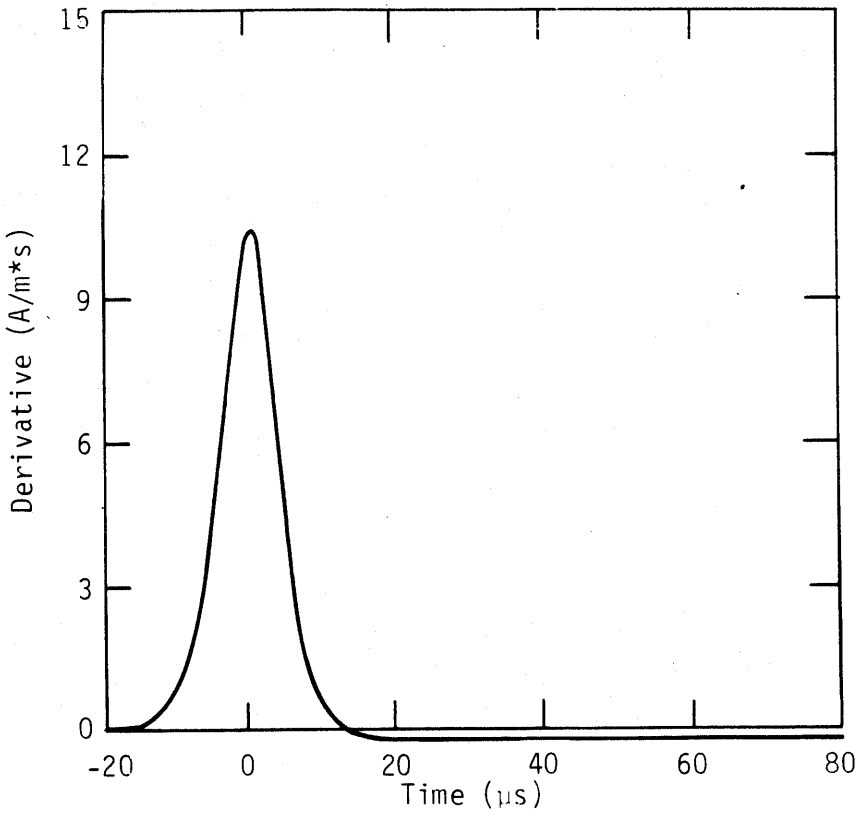

Figure 22. Time derivative of current described by Equation 7.

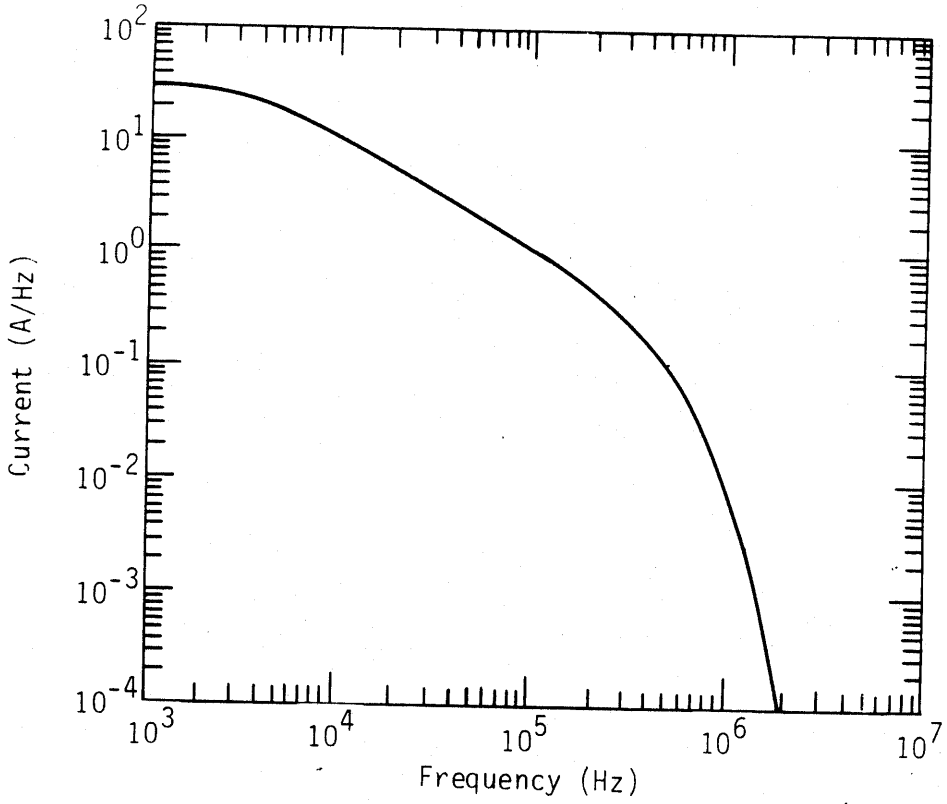

Figure 23. Frequency spectrum of current from a Fourier transform of Equation 7.

The waveform of lightning discharge currents, for discharges near and on aircraft, varies considerably in magnitude, rise time, and duration. The environment governing the parameters of the initiation of the discharge has so many variables acting over such a large volume of space that the parameters of the discharge are usually considered random variables. Experimental programs whose purpose is to measure lightning parameters are usually designed to gather empirical evidence on the magnitude and frequency of occurrence of various parameters important for describing the threat caused by lightning discharge. The data, from a program of this sort, are then often subjected to a number of statistical tests. These tests can determine the likelihood that a particular parameter, such as current rate of rise, will occur during a given set of circumstances, such as flight level of the aircraft relative to the freezing level or to the precipitation density at the aircraft's location. If there is no coherent theory of the phenomena under study, such as

lightning initiation, such a procedure is good scientific procedure. The danger of these empirical techniques, however, is that the limits imposed by nature on lightning are masked by the statistical manipulation.

In an empirical study, the data are generally fit to a specific probability distribution for which statistics are understood: a log normal distribution, for example. This distribution is then used to determine the probability of a given current magnitude. The danger inherent in such manipulation is that this type of distribution has infinite extent. That is, no matter how small a likelihood is tolerated for the probability of a given threat current, the distribution will predict a large current to go with it, even if the current greatly exceeds the data range that generated the distribution.

III. INTERACTION

In addition to differences in the electrical environment produced by the lightning and HEMP, differences in the efficiency with which these environments interact with aircraft also exist. Each threat interacts differently with objects such as an aircraft to produce currents in their electronics. Since the high frequency signals of HEMP do not generally produce the large, low frequency currents that cause the physical damage associated with lightning interaction, these low frequency effects (although briefly described) will not be considered in the comparison of HEMP and lightning. In this section, the physical differences between lightning's and HEMP's interactions with an aircraft are described; some of their differences are also illustrated by using simple geometric models. This research project, however, did not consider all the details associated with a real aircraft interacting with either lightning or HEMP because the research required was beyond the scope of this work.

1. PHYSICS OF INTERACTION OF LIGHTNING AND HEMP WITH AIRCRAFT

a. Direct Strike Lightning--Direct strike lightning and incident electromagnetic waves like HEMP and waves from nearby lightning strikes interact with aircraft in physically different ways. While understanding the basic physics of the interaction of a lightning strike with an aircraft is still in its very early stages, a qualitative description of the interaction process with direct strike lightning can be presented. When an aircraft enters a thunderstorm, it is under the influence of an electric field which by polarizing the aircraft induces image charges and causes currents to flow on the aircraft's skin. If a leader streamer approaches the aircraft, those fields become much larger, particularly around sharp corners and edges near the streamer. As the local fields approach a level of about 3 MV/m or lower altitude, the air begins to break down in the field enhanced region and forms a corona. This corona exhibits nonlinear characteristics which complicate the electromagnetic behavior of the aircraft under the influence of the nearby streamer. A very qualitative description of the macroscopic coronal behavior is that it exhibits the conductivity of wood until the fields begin to exceed approximately 3 MV/m. At this point, the conductivity of the air is increased substantially by

electrons produced through avalanching on a time scale that is short when compared to lightning's. The increased conductivity tends to clamp the field at the 3 MV/m value.

As the leader attaches to the aircraft, coronal activity increases and a channel forms. As current flows through the channel, the air gets hotter and the number of active physical processes increases dramatically. Hydrodynamic expansion, radiative transfer, thermal conduction, joule heating, and field emission from the metal surfaces all play a part in developing the channel that in turn forms the current carrier for the lightning direct strike.

The system of clouds, channel, and aircraft should be viewed as an electrical circuit. Initially, because the channel is cool and narrow, it is both resistive and inductive; consequently it limits both the current and its rate of rise. As the lightning channel forms and as the return stroke current flows, the channel becomes hotter and larger in diameter. These increases, in turn, diminish the resistance and inductance of the channel, allowing more current to flow more rapidly. The channel expansion obeys a complex set of simultaneous differential equations that determine channel growth that is controlled by phenomena like radiative heat conduction and complex air chemistry. Since the aircraft, itself, is part of the electrical circuit under examination, it must be considered when developing an understanding of the entire interaction problem. Consequently, researchers must include both the effect of the aircraft on the formation of the lightning channel as well as the effects of the channel formation and the corona surrounding the aircraft when they analyze the current flow's effect on the aircraft, itself. In other words, the complete interaction of direct strike lightning with an aircraft is a nonlinear interaction of a large current with the air, the aircraft and the region of the thunderstorm local to the aircraft. Many of the details of the physical processes, however, are not completely understood because of the range of length scales in the problem and the large variation in the physical variables. The problem is not susceptible to either brute force numerical or to empirical techniques.

One way the surrounding corona and the attached channels manifest themselves is by altering the resonant frequencies of the aircraft. These resonant (or natural) frequencies of a structure are useful in describing the electromagnetic response of a conducting or partially conducting body. In

a normal electromagnetic scattering problem, such as HEMP, the natural frequencies are functions solely of the geometry and the material of the scatterer. This functionality neatly separates the natural frequencies of the scatterer from those of the exciting field which, of course, results in a linear problem. Since the corona and channel shift (which in some approximation may be treated as conductors loading the aircraft) the resonant frequencies, (as will be shown later in the section), in a way that depends on the current in the channel, that separation is no longer valid and the problem becomes nonlinear. Because the natural frequencies (the geometry of the conducting body in question) now depend on the driving current, that is, the lightning, the analysis techniques used for the direct strike problem must be used with care.

The difficulty caused by the large range of length scales deserves further comment. The interaction of electrical conductivity produced by the charged particle densities and the local electric field, that produces the collisional ionization dominating the production of the electrical conductivity, occurs on length scales of the order of 0.0001 m (Ref. 40). The macroscopic interaction problem determining those local electric fields is of the order of tens of meters and includes the aircraft and the lightning channel, as well as the charge stored in the surrounding clouds. This combination gives a range of length scale of at least 10^5 per dimension. Electromagnetics codes designed to solve less difficult linear electromagnetics problems can handle length scale variation ratios on the order of 10^2 per dimension. However, even with subgridding techniques, the problem requires more zones for its solution than are now available in the state-of-the-art finite difference codes. Additionally, the problem would also require simple analytical or semi-empirical methods to circumvent the remaining numerical problems.

In a comparison of HEMP and lightning, high frequency signals affecting system electronics should also be considered. It must be noted, however, that the total energy content delivered to an aircraft by a lightning direct strike is much larger than that delivered by HEMP. Lightning's energy is mostly in the sub-MHz frequency band and consequently does not couple to system electronics as efficiently as higher frequency signals. Although low frequency energy can significantly damage an aircraft, that damage is likely to be

structural or direct, rather than indirect effects on electronics. However, indirect effects, usually associated with super-MHz frequencies, can cause far more subtle difficulties such as upset and damage to individual electronic components. Direct damage from lightning, of course, may be quite severe; there are, in fact, documented cases of fuel tank explosion and complete loss of flight control systems (Ref. 41). Since the interaction of HEMP seldom directly affects the aircraft, the subject of direct effects does not need to be explored further for a complete comparison of HEMP and lightning.

b. Free Field HEMP Interaction--HEMP will be experienced by an aircraft as an electromagnetic wave. For all intents and purposes, HEMP will occur as a plane wave and hence will be uniform in amplitude and phase. The amplitude of the time-varying electric and magnetic fields will be related by $E/H = Z_0$, where Z_0 is the impedance of free space (377 Ω), and will be transverse to the wave's propagation direction. These varying fields will induce currents on the aircraft making it act as an antenna. Additionally, cables and electronic equipment in the aircraft will also act as antennae and will develop voltages due to fields penetrating the apertures (seams, dielectric windows, radomes, etc.). Generally, these internal fields will be reduced by the shielding effects of the conducting aircraft. Particularly for the lower frequencies, the surface currents induced on the metallic skin will produce fields that will tend to cancel the HEMP fields which caused them. However, for higher frequencies (that is, wavelengths that are small compared to the aperture in question), this shielding is minimal. Cables might pick up fields from a number of apertures; all of which can, for particular angles of incidence, drive the cable in phase because of the plane wave nature of HEMP. This in-phase drive is in contrast to direct strike lightning where the phase of the fields driving the aperture fields is determined by the flow of current along the fuselage.

In its basic behavior, the interaction of an unattached, but otherwise nearby, lightning strike will be generally similar to that of HEMP. The electromagnetic wave will be less planar, but otherwise similar if the aircraft is in the far or radiation zone. If the lightning strike is both closer to the aircraft and in the inductive zone of the channel fields, then the analysis

becomes more complicated and would require a multipole expansion to compute the fields.

The complex nature of air reacting to high electromagnetic fields is important in the interaction of incident electromagnetic waves produced either by HEMP or by nearby lightning strikes with an aircraft; these are nonlinear processes. They are not as integral to the interaction phenomenology as they are in the direct strike problem. Examination of the literature of HEMP, for example, (Ref. 42) reveals a high concentration of work on the purely electromagnetic aspects of the interaction problem. Such problems, of course, must be addressed. Later in this chapter, illustrations of the interaction of plane (and one example of nonplanar) illumination of simple objects are used to show how such interaction problems may be solved. However, the problem of HEMP or lightning interaction with a real aircraft has not yet been solved.

After establishing the existence of nonlinear behavior in certain free field interaction problems, the interaction of free field electromagnetic waves involves only a solution of Maxwell's equations for the boundary value problem of interest. While this solution may be a very difficult undertaking, it is certainly a different problem from the solution of the equations required to describe natural lightning. The natural lightning procedure involves simultaneously solving: Maxwell's equations along with fluid equations; equations governing air chemistry; and, the equations of radiative transfer. Even numerical solution of all of these equations have been achieved only for very limited problem geometries. (See, for example, Ref. 43, for a survey of the air breakdown literature.)

c. Rationale for use of D and H in the comparison--When comparing electromagnetic threats to aircraft it necessary to compare those fields which are important in determining the penetration of the fields into the aircraft. Those fields are the normal electric field or equivalently the surface charge density and the tangential magnetic field or equivalently the surface current density (Ref. 44). Certainly, it is desirable to choose only the dominant threat for the comparison if one exists. The relative effectiveness of the two types of threats at penetrating the aircraft is indicated by the wave

impedance Z = E/H at the surface of the aircraft and the surface charge and current are of equal importance when Z = 377 Ω, the impedance of free space. For an incident plane wave, like HEMP or nearby lightning, the wave impedance is always 377 Ω. For direct strike lightning the impedance may vary and must be estimated for the particular problem.

In the upper limits of the parameters describing direct strike lightning the impedance may be calculated directly by dividing the largest expected value of E by the largest expected value of H. The upper limit of E is the breakdown value for air, E = 3E6 V/m. For the largest expected value of H we are forced to use the reasonable worst case current, 100 kA described in section II, subsection C and assume it is propagating along a 1 m radius cylinder. The resulting impedance is about 200 Ω, indicating a dominance of the surface charge density. A review of the natural lightning data gathered on the surface of the F-106B (Ref. 16) indicates that the impedance is about 2,000 Ω, indicating a dominance of the surface charge.

Since both surface charge and current are important to the process of coupling energy into the aircraft both must be considered when comparing electromagnetic fields.

In summary, HEMP and lightning can interact with aircraft differently. Both can interact through an electromagnetic wave, which may be viewed as a displacement current $J = dD/dt = \varepsilon\, dE/dt$. In addition, lightning, for a direct strike, can pose a qualitatively different threat because of the conduction current. This effect is most important at lower frequencies, since the strength of the displacement current effects are proportional to the time derivative of the fields; consequently they are unimportant at low frequencies. Significantly, this expectation is confirmed by a detailed analysis that will quantify what "high frequency" means in this regard.

2. SAMPLE INTERACTION PROBLEMS

The remainder of this chapter is a compendium of interaction models for both the free field environment and the direct strike problem. The compendium

has several canonical problems representing the interaction of HEMP and lightning direct strikes. These problems possess certain simple geometric objects that model certain salient characteristics of aircraft. These models used to quantify the threats caused by HEMP and lightning have three frequency ranges of interest:

- Low frequencies, those below the resonant frequencies of an aircraft, typically below 2 MHz;
- Intermediate or resonant frequencies; typically 2-20 MHz;
- High frequencies, those in which the fine details of aircraft geometry (such as the shape and size of apertures, become important), typically above 20 MHz.

In the resonant or intermediate frequency range between 1 and 20 MHz, the response of the aircraft is dominated by the gross structural resonances of the aircraft and may be quite complicated. The various models to be used are shown in Table 1.

TABLE 1. INTERACTION MODELS TO BE PRESENTED.

		Model		
		Frequency Domain		
Effect	Variable	Low	Medium	High
HEMP/Nearby	Current	Slab	Sassman	Slab, GTD
Direct Strike	Current Charge	Continuity Ellipsoid	T-Line T-Line	

3. MODELS FOR HEMP AND NEARBY LIGHTNING STRIKES

a. Slab Model--In other research (Ref. 22), it was assumed that the fields produced by HEMP on the surface of an aircraft were just the incident fields themselves. However, a better approximation, that still requires very little calculational effort, is to allow for the reflection of those incident fields from the aircraft surface. In the optical or high frequency

approximation, only local reflection is important; consequently, the surface of the aircraft may be modeled as a perfectly conducting slab. The problem of a plane electromagnetic wave reflecting from a plane surface is, of course, a typical textbook problem in electromagnetics (Ref. 32). The magnetic field on the conductor surface is just twice the incident field. This simple model follows the waveform and therefore has the same spectrum as the incident pulse. The magnitude is only doubled. From the results of more complex analysis used to work a more detailed problem (Ref. 45), it is found the ratio of incident field to surface field of two is correct for the low frequency limit. However, in the resonant region of the structure under consideration the ratio is a very complicated function of frequency. (These complicated functions will be fully discussed in the next subsection.)

b. Sassman Model--For the intermediate, or resonant frequency regime the charges and currents on a finite cylinder are computed using the solution of Sassman (Ref. 46). Incident fields are computed using both HEMP plane waves and the incident fields from a tortuous lightning channel (Refs. 47, 48). In particular, the lightning waveform introduced at the end of Section II is used to maintain a reasonable high frequency behavior of the lightning current.

The Sassman model assumes a right circular cylinder; and although end effects are not neglected, they are approximately treated. The model further assumes that the incident electromagnetic field is a plane wave incident normal to the surface, with the E vector parallel to the cylinder axis. This situation constitutes the most dangerous polarization threat. This model also requires that the lightning or the HEMP source is sufficiently far away so that the exciting field may be considered uniform over the cylinder. It would be simple to generalize the model to include non-normal incidence. This was not discussed in Sassman, however, and is not necessary for the purposes of this study because normal incidence would generally constitute the worst case threat scenario. Results of the model were compared with those reported by Sassman and the agreement was excellent and are shown in Figure 24.

The solution of Sassman (Ref. 46) is not presented in closed form; rather, a system of finite difference equations for positions along the cylinder and

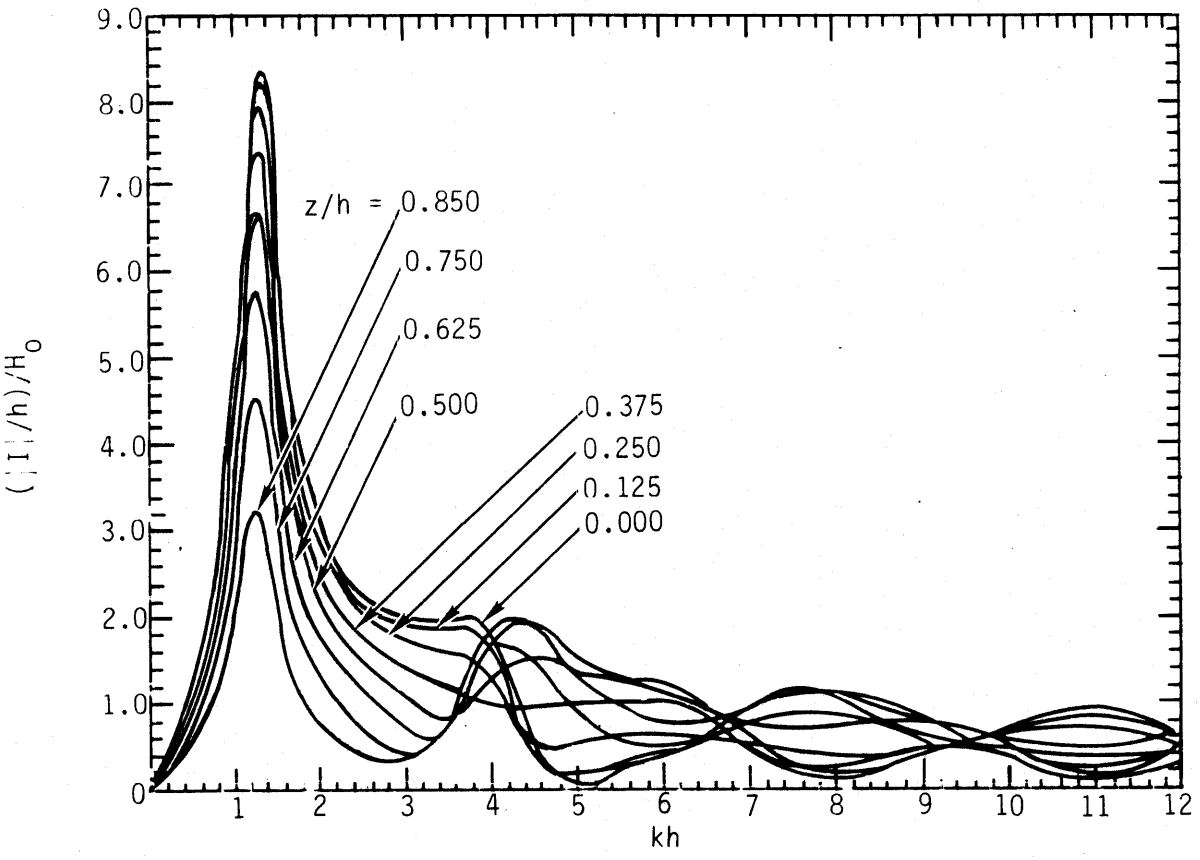

Figure 24. Our calculation of cylinder response function which is virtually identical to that calculated by Sassman.

at the end of the cylinder is given. These must be solved for the current (in the frequency domain) flowing at these positions.

4. HIGH FREQUENCY APPROXIMATION--GEOMETRIC THEORY OF DIFFRACTION

In order for this study to be complete, a model illustrating the behavior of fields with wavelengths of the order of the diameter of the aircraft fuselage is included for incident plane waves. This model is useful for understanding the effects of shadowing on measurements of high frequency fields. For subresonant frequencies, the surface currents and charges are relatively independent of the angle of incidence. For wavelengths shorter than the fuselage diameter shadowing occurs and the Geometric Theory of Diffraction can be used to calculate the effect of shadowing on the measured fields (Ref. 49).

As shown in Figure 25, a cylinder illuminated broadside has an illuminated and shadowed side, as in ordinary optics. There is also a diffracted or creeping ray contribution. Consequently, although the fields are smaller on the shadowed side, they are not absent as one might expect for an illumination at frequencies associated with light. In Figure 25, the cylinder is illuminated broadside by a source; and, using GTD, the field at point P in the optical shadow region may be calculated. A ray might travel along L_1, be diffracted along L_2 and reach P over path L_3. In GTD the "creeping" ray is assumed attenuated exponentially along L_2, that is through angle γ_3. The exponential attenuation per unit length L^2 is given by $e^{-\chi_p L^2}$ where:

$$\chi_p = \frac{Im(\mu_p)}{a} \tag{9}$$

where μ_p is a solution of (Ref. 50):

$$H_\mu'^{(1)}(ka) + i\,\overline{C}\,H_\mu^{(1)}(ka) = 0 \tag{10}$$

where $\overline{C}$ bar is the normalized surface impedance of the cylinder and the $H_\mu^{(1)}(ka)$ is a Hankel function of the first kind. Results for the surface current on the surface of a perfectly conducting cylinder illuminated by a plane wave

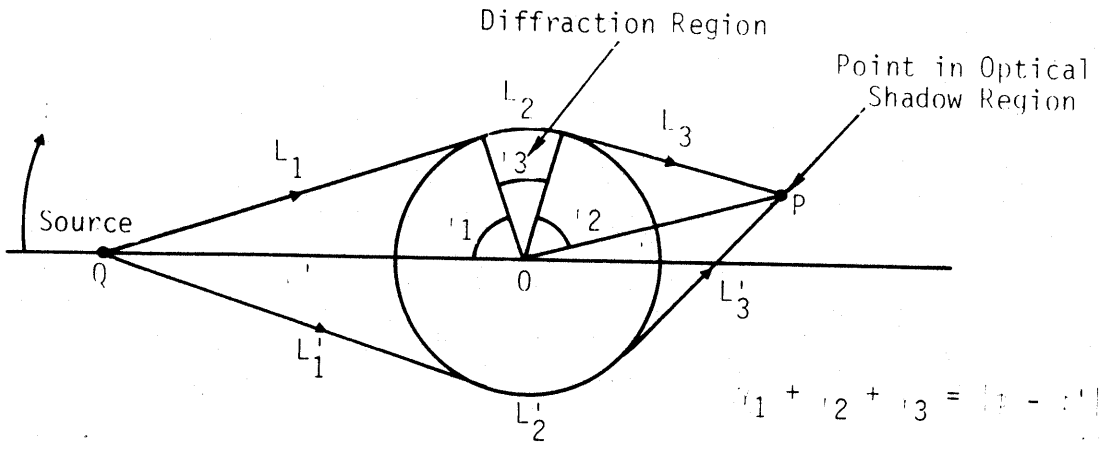

Figure 25. Geometrical interpretation of field in shadow region (Ref. 50).

for a cylinder of radius a = $\lambda/3$ is shown in Figure 26. The illuminated and shadow sides are distinguished by the lack of significant surface current on the shadow side. Diffraction accounts for the smooth transition between the shadowed and illuminated regions.

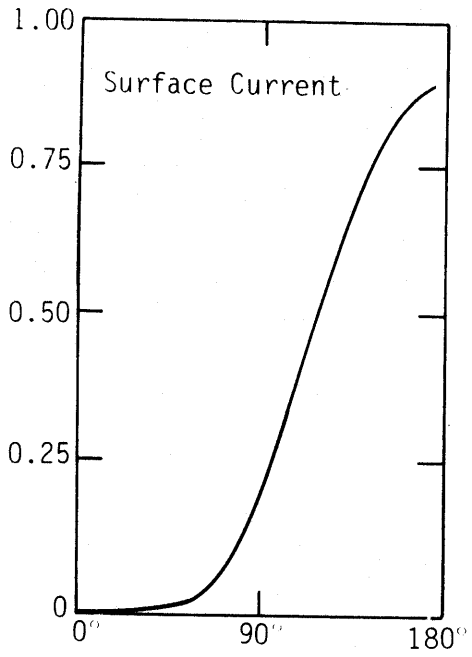

Figure 26. Normalized surface current on a cylinder illuminated by a plane wave at ϕ = 180° (Ref. 51).

5. MODELS FOR DIRECT STRIKE LIGHTNING INTERACTION

For direct strike lightning, a current is injected onto the aircraft skin and the lightning strike current actually flows along the aircraft skin. The simplest model (the one used in Refs. 11 and 22) assumes a continuous current density around the circumference of a cylinder. In this static field approximation, the lightning current is assumed to flow uniformly on the surface of a cylinder. Therefore, the current density, J(t), is related to the incident lightning current I(t) by:

$$J(t) = \frac{I(t)}{2\pi r} \tag{11}$$

The surface magnetic field is then given in magnitude by:

$$H(t) = J(t) \tag{12}$$

and is perpendicular to the surface current.

On an actual aircraft, the low frequency current would be divided by gaps in the skin. The current would then flow along the least resistive path, causing high surface currents and, consequently, high magnetic fields in those regions where the surface current is constrained. As the frequency of the current rises and approaches the resonance region, reflections from various parts of the aircraft become more important in the interaction problem. As shown in a later section discussing transmission line theory, these reflections can be modeled by using this theory. However, the unipolar nature of the lightning channel current leads to the buildup of charges on parts of the aircraft. The magnitude of the local charge density is typically related to the local radius of curvature as may be seen by examining the following simple model.

Consider an ellipsoid with overall length 20 m and diameter 1 m. These dimensions are roughly those of the fuselage of an F-106B. Such an ellipsoid with a given charge on it has a surface charge density as a function of position described by (Ref. 52) as:

$$\sigma = \frac{q}{4\pi abc} \frac{1}{\sqrt{\frac{x^2}{a^4} + \frac{y^2}{b^4} + \frac{z^2}{c^4}}} \quad (13)$$

q is the total charge on the ellipsoid

a = b = 1 m are the smaller radii

c = 10 m is the long radius of the ellipsoid

σ is the surface charge density

The related normal electric field is given by:

$$E_n = \sigma/\varepsilon_0 \quad (14)$$

The total charge on the ellipsoid may be computed by integrating the current injected onto the ellipsoid minus the current leaving the ellipsoid. In this case, the entering and leaving current are assumed to be the current of Equation 7 of the previous chapter; however, the current reducing the charge is delayed by the time it takes light to travel from one end of the ellipsoid to the other, or about 60 ns. The resulting normal electric fields are shown in Figure 22 where values for the beltline of the ellipsoid and the end of the ellipsoid are given as functions of time. The result of a hand integration of the $\dot{D}$ measurement for flight 80-018 of the NASA F-106B is also provided for comparison. Note that the measured value is limited by the value at which air breaks down in a uniform field. The results of this simple model clearly show that nonlinear or corona effects can occur on the F-106B.

Note, also, that the charge density at the beltline is proportional to $(ac)^{-1}$ and the charge density at the end of ellipsoid is proportional to $(c^2)^{-1}$. The proportionality of the charge density to the square of the local radius of curvature is a general result, indicating that coronal effects are most likely to occur near sharp points or edges.

Also shown in Figure 27 are a number of important values for $\dot{D}$, as well as the time rate of change of D. The maximum values for $\dot{D}$ attained in the simple model of this section are given for both the beltline and the end prediction. The maximum value in the sample waveform is also given. This sample waveform

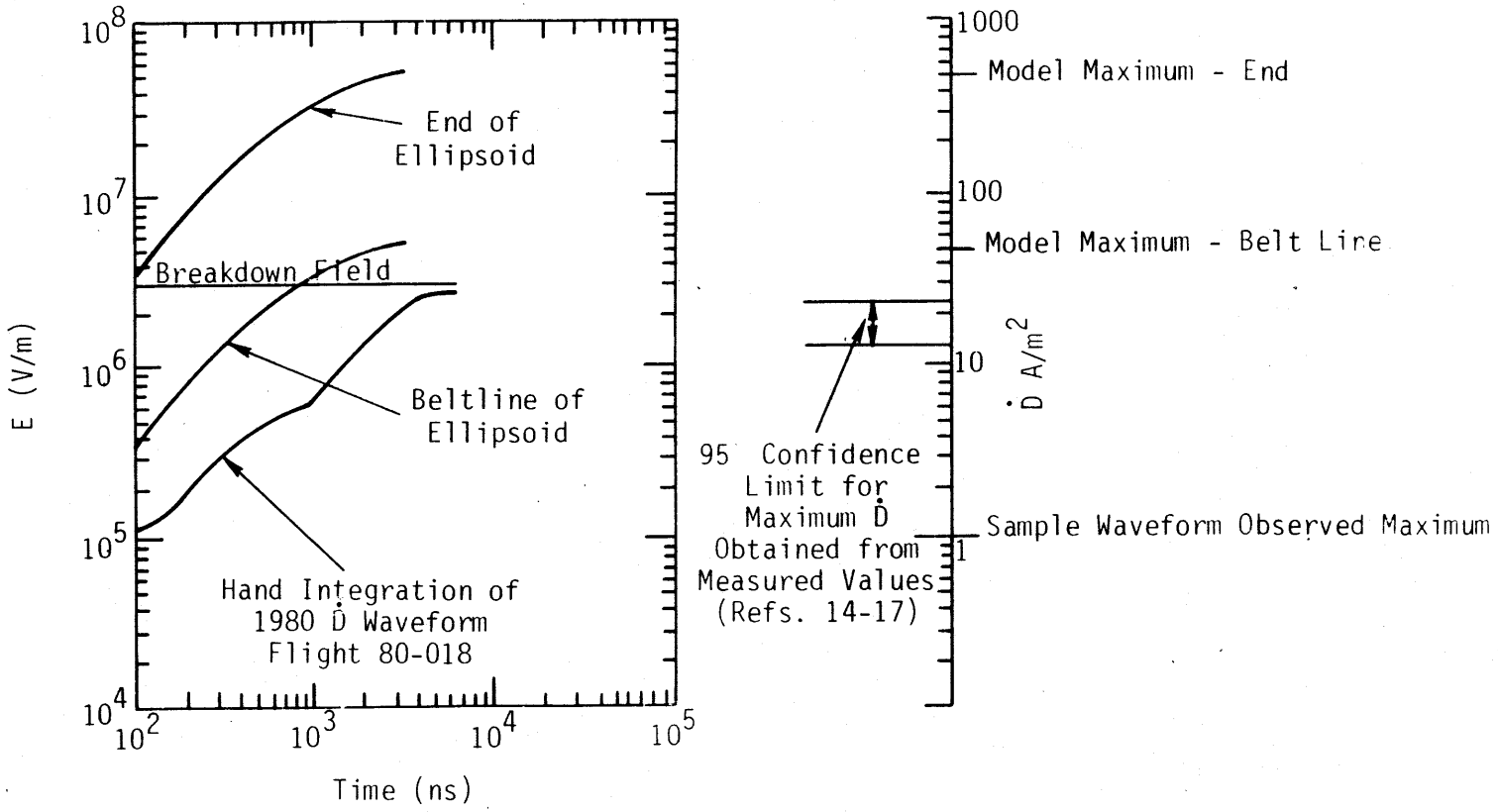

Figure 27. Surface charge characteristics for ellipsoid model and F-106B data.

was chosen because it had the largest area, or was likely to give the largest $\dot{D}$ rather than the largest $\dot{D}$. Finally, values for the confidence limits for the maximum of $\dot{D}$, are derived from the measurements on the F-106B taken in 1980-1982.

Although an ellipsoid is a poor model of an aircraft, the following simple analysis of a set of transmission lines allows a better assessment without resorting to a large numerical calculation. A discussion of this model follows.

6. TRANSMISSION-LINE MODEL FOR LOW AND INTERMEDIATE FREQUENCIES

A transmission-line model may be developed for the direct strike case which is valid for intermediate as well as low frequencies. This model is especially simple in the case of the F-106B because of its delta-wing configuration. The wings and tail may be modeled as transmission lines attached to the end of the transmission line representing the fuselage; this model is an excellent representation of the natural modes of the aircraft. This simple model may be justified a posteriori by comparison with the results of more sophisticated but costly models. For example, the models of Taylor and Crow (Ref. 53) solve a linear system after numerically evaluating the Sommerfeld integrals for a representation of the aircraft as an assembly of cylinders. The Singularity Expansion Method (SEM) formalism is then employed to discuss the natural modes of the system. A glance at the figures depicting the modes found show that they are qualitatively as would be expected on a system of transmission-lines, the currents being nearly sinusoidal along individual structures (wings or fuselage). Similar sinusoidal current distribution is seen, for example, in the work of Lin and Cardaro (Ref. 54) and we may assume that this behavior is both typical and general.

Therefore, it should not surprise anyone that a model that represents a wing by one or two transmission-line elements gets answers that differ only slightly from a model that employs many cylinders whose properties require numerical integration for determination. Given the uncertainties introduced by corona discharges, the extra complexity of these more sophisticated models is not justified for the present problem.

The multi-transmission line may be conveniently analyzed through the formalism developed in the well-known "BLT" paper (Ref. 55); once the topology is determined, the usual transmission-line impedance matrices may be incorporated into the supermatrix along with the connectivity matrix and the system solved for voltage and current supermatrix. From these branch currents and node voltages, the voltages and currents at any point may then be found, and from charge continuity the surface charge density at any cross section may then be calculated. If analytic results are not required, any circuit code such as SCEPTRE or SPICE may be used, treating the transmission lines as either two-ports or else using current-dependent voltage sources.

Following King (Ref. 56), the current at any point along the aircraft fuselage (represented here as the main transmission line) is given by:

$$i = \frac{V\,(\exp(-gz) - \Gamma[\ell]\exp(-g(2L-z)))}{\{Z[a]+Z[\ell]\}\{1-\Gamma[\ell]\,\Gamma[t]\exp(-2gL)\}} \qquad (15)$$

where $L = 21.55$ m is the length of the aircraft fuselage (Ref. 57); $Z(a)$ and $Z(\ell)$ are the impedances of the aircraft and lightning channel, respectively; $\Gamma[\ell] = (Z[\ell] - Z[a])/(Z[\ell] + Z[a])$, the reflection coefficient at the attachment point; $\Gamma[t] = (Z[t] - Z[a])/(Z[t] + Z[a])$ is the reflection coefficient at the termination into an impedance $Z[t]$; and V is the voltage source driving the system. The current in the lightning channel, in the absence of the aircraft, I, may be related to V by $V = 2I/\{Z[\ell] + Z[t]\}$, with $Z[t] = Z[\ell]$ if $Z[\ell]$ is the channel characteristic impedance. Depending on the assumed stroke path along the aircraft, various expressions for $Z[t]$ occur. For example,

$$1/Z[t] = 1/Z[\text{exit}] + 1/Z[\text{wing}] + 1/Z[\text{wing}] + 1/Z[\text{tail}] \qquad (16)$$

for an attachment to the nose boom with an exit from the fuselage tail. Often the exit is from the tip of the tail or a wing. The fin in question is, then, in series with the exit channel, for example:

$$1/Z[t] = 1/\{Z[\text{exit}] + Z[\text{wing}]\} + 1/Z[\text{wing}] + 1/Z[\text{tail}] \qquad (17)$$

for an exit from a wingtip. Also $Z[\text{exit}] = Z[\ell]$ can be expected.

This simple model does a surprisingly good job of reproducing the aircraft resonances. The lowest resonances are (Ref. 58) at 8, 13.5, 16, 19.4, and 23.6 MHz, attributed alternately to fuselage (8, 16, 23.6 MHz) and wings and tail (13.5, 19.4 MHz). In the transmission line model, the fuselage length of 21.55 m gives a resonance at 7.8 MHz, with higher harmonics at 15.6 and 23.4 MHz. Similarly, when the span of the F-106B is 11.68 m (Ref. 57), the full-span resonance is 12.84 MHz, and the fuselage plus wing resonance at 20.6 MHz. To include the lowest spanwise resonance, the simple model described above would have a transmission line extending from wingtip to wingtip, as sketched in Figure 28a. This corresponds to a folded-dipole model for the wings. Similarly, Figure 28b shows a model that takes better account of the delta-wing planform, and should more accurately depict the higher frequency resonances if this is required. Here S denotes the span and ℓ the fuselage length, while T_W, T_F, T_L, T_S denote the transmission line corresponding to the wing, fuselage, lightning channel, and rear wing span, respectively. This model allows differential-mode propagation along the fuselage as well as the common mode of the simple model, thus allowing the estimation of current density variation around the fuselage and on the wing surfaces. With the aid of computer algebra programs, the six-coupled-transmission-line model may be solved analytically for use in computer codes.

Because of this ability of the transmission line model to reproduce the principal resonances of the wire-mesh aircraft models, it should do a similarly capable job of field and current prediction.

7. SUMMARY

In this chapter a series of simple models were used to describe the salient concepts involved in the interaction of HEMP and direct strike lightning with aircraft. Physically, these two threats interact with aircraft in different ways. HEMP as an incident plane wave causes currents to flow and charge to collect on the aircraft primarily by polarization of the aircraft by the incident fields. For direct strike lightning, the current actually flows on the skin of the aircraft. In addition, large charge densities form in the direct strike lightning case because of the unipolar nature of the injected

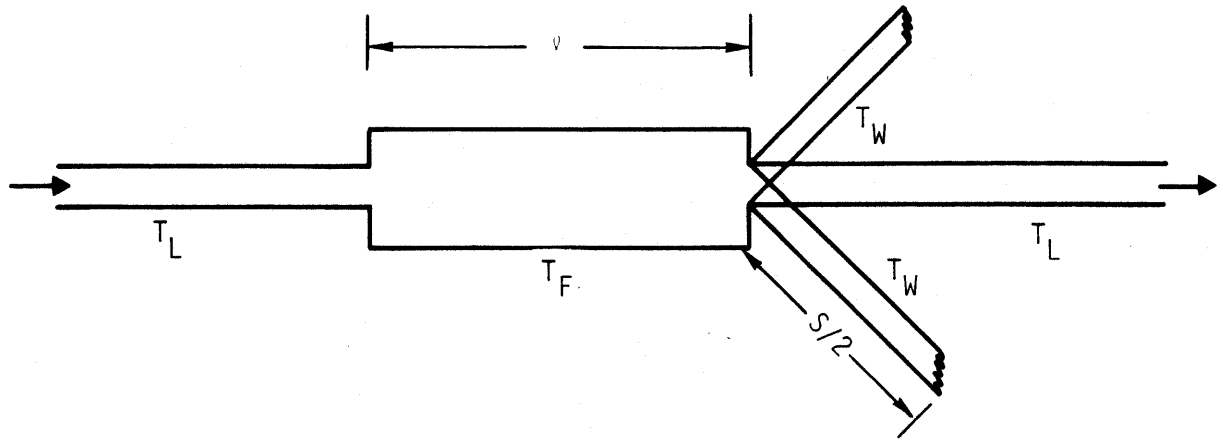

a) Simple transmission line model of F-106B. This model accurately reproduces the fuselage resonances.

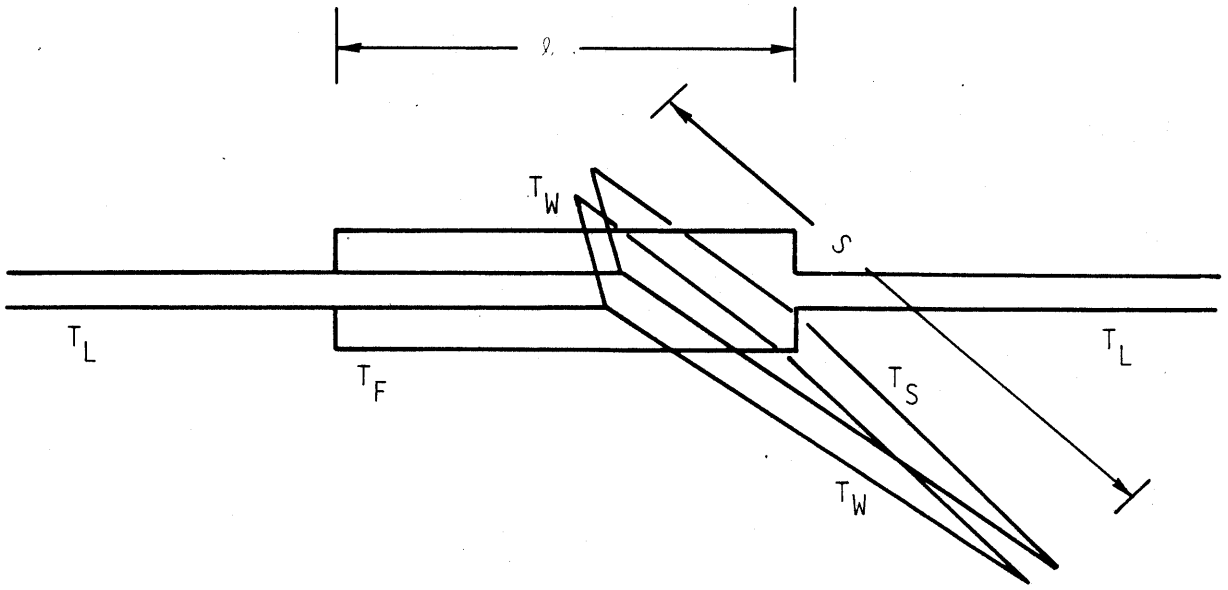

b) More complicated transmission line model to include the wing resonances. Tail could be included in a similar fashion

Figure 28. More sophisticated transmission-line model for lightning direct strike. The models show attachment to the nose (boom) of aircraft and channel exiting tail region; other cases vould be similar.

current. Consequently, an enveloping corona plays a much larger role in the interaction of lightning with aircraft than it does in HEMP with aircraft. Finally, since the attached lightning channel affects the electrical response of the aircraft, it must also be considered in a model of the interaction of lightning with an aircraft.

The various models used to describe the important features of lightning and HEMP with an aircraft are summarized in Table 1 (Section II, paragraph 2). These models are needed in the various frequency ranges of the interaction process. Their important figures of merit are the current and charge densities on the model surface as functions of position. The simple models will be used to compare lightning and HEMP in the next chapter.

IV. COMPARISON

The electromagnetic environments in the form of an incident plane electromagnetic wave for HEMP and an incident wave and injected current for lightning were established in Section II, while Section III discussed computing the aircraft's response to electromagnetic waves and injected currents. In this section, the results of Section II will be combined with the methods of Section III to characterize the threats of HEMP and lightning.

Below 1 MHz, the aircraft reacts as it would to a static field or current. Although indirect affects on system electronics do occur, direct effects like pitting, radome penetration, or flashover in fuel tanks are more likely sources of physical damage than aircraft upset. Since the energy content of lightning is considerably greater than HEMP, the likelihood of direct (physical) damage is, of course, far greater for lightning than for HEMP.

The resonant region is characterized by certain frequencies (the natural frequencies) very efficiently interacting with the aircraft. For a typical electromagnetic scattering problem, where a plane's electromagnetic wave interacts with a conducting body, the natural frequencies are functions only of the geometry of the scatterer. However, as the discussion in this section will clearly show, the natural frequencies are shifted by the presence of the corona and the lightning channel. Such a shift complicates the comparison of lightning and HEMP in the resonant frequency regime.

The high frequency region, above about 10 MHz, is characterized by wavelengths comparable to small structural features of the aircraft. In other words, details of the aircraft's geometry, such as apertures, fuselage cross section, and engines are comparable in size to the threat wavelengths. To be valid in this frequency range, then, electromagnetic scattering solutions must be capable of treating these details. For plane wave interaction, numerical solutions capable of resolving 1 m (wavelength of 300 MHz) while treating some specific details have been accomplished by using special numerical techniques. However, these numerical techniques are usually limited to early times, while the analytic solutions have been limited to solutions of

particular parts of the overall geometry, such as a solution for an isolated aperture. For direct strike lightning, the high frequency characteristics of a lightning discharge are not fully understood; consequently, the combined interaction of direct strike lightning and aircraft at high frequencies is also not understood.

This section discusses some evidence for the shift in resonant frequencies and assesses the importance of the shift in natural frequencies necessary for the comparison of HEMP and lightning. Two comparisons of HEMP and direct strike lightning are, then, shown. The first presentation uses the continuous current model for direct strike lightning (Section III, paragraph 1) and the slab model (Section III, paragraph 4a) for HEMP. These simple models are pertinent because they are similar to those used by other researchers (Ref. 24). In this comparison a region of uncertainty is also shown to indicate the difficulty in assessing the resonance region of the spectrum.

The second comparison of surface currents will apply the Sassman model for HEMP (Section III, paragraph 4b) to a simple cylinder and the transmission line model (Section III, paragraph 6) for direct strike lightning. Finally, at the end of the section, conclusions about the relative threats to aircraft by HEMP and lightning are presented.

1. EFFECT OF NATURAL FREQUENCY SHIFT ON THE COMPARISON

The natural frequencies of the F-106B, used in a series of lightning experiments, have been determined from a variety of of methods (Ref. 58). One of the methods is to use Prony analysis to extract the natural frequencies from measured waveforms. This analysis fits an electromagnetic sensor waveform f(t) with a series of the form:

$$f(t) = \sum_{i=1}^{N} A_i \, e^{s_i t} \tag{18}$$

where the s_i represents the complex natural frequencies. Such a method was used to extract the F-106B natural frequencies from nearby strike data and portrays the natural frequencies of the aircraft with no attached channel. These data are plotted (Refs. 58, 59) with the circles in Figure 29. In

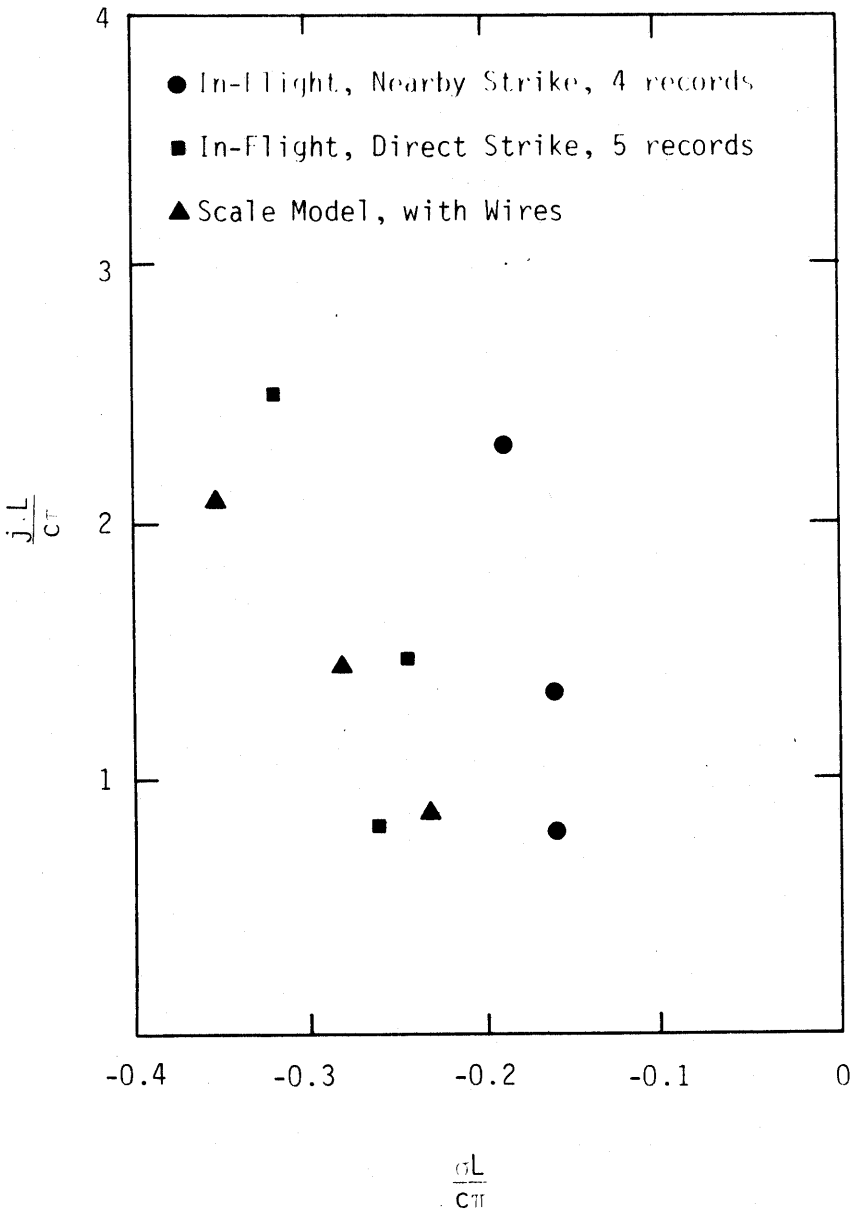

Figure 29. Shift in natural lightning due to the loading by the lightning channel.

Figure 29, in order to show these shifts, the results of a Prony analysis of the data for an aircraft having an attached channel and surrounding corona are plotted as the squares. The natural frequencies are shifted to represent a more dissipative structure than a bare aircraft.

To reproduce this phenomena in the laboratory, a simple scale model of the F-106B was constructed; wires were attached to represent the effects of the channel (Ref. 59). In Figure 29, measurements of the natural frequencies of the model system are shown by the triangles. The results shown in Figure 29 demonstrate qualitatively that the natural frequencies and, therefore, the electromagnetic response of the aircraft is distorted by the presence of the channel and the corona.

The importance of this shift in natural frequencies may be seen by examining the curves in Figure 30. This figure shows a hypothetical transfer function from one exterior environment to an interior system. Two possible exterior environments are superimposed on the transfer function. The threat to the system is found by multiplying the transfer function with the threat environment. For example, suppose environment A is HEMP and environment B is lightning. Because environment A has peaks at the same frequencies as the transfer function, and environment B has peaks near the minima of the transfer function, environment A results in far higher currents at the interior system. For the choice of environments given above, HEMP would be the dominant threat. The opposite conclusion, however, would be drawn if environment A were lightning and environment B, HEMP. Since there is no way to know beforehand which environment will couple most efficiently to a particular electronic system, it is not clear which threat will dominate for a particular electronics box within the resonant region of the aircraft. Examination of data acquired by measurements of current densities and charge densities on aircraft in HEMP simulators (Ref. 60) or exposed to lightning (Refs. 15-17) reveals that the electromagnetic variables do swing significantly in the resonant region of the aircraft.

When the threats of HEMP and lightning are compared, the uncertainty in the dominant threat shows up as a region of uncertainty.

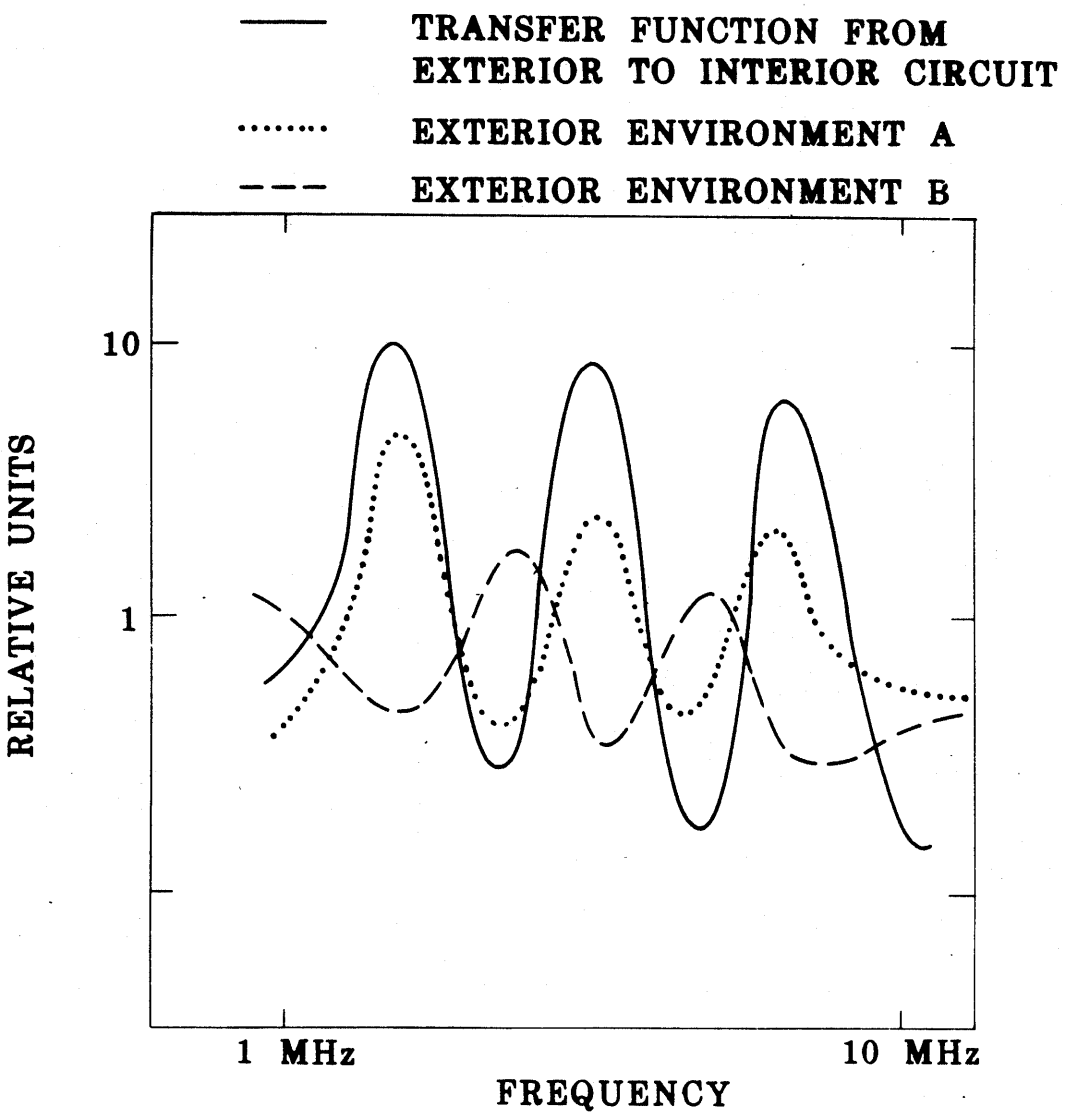

TRANSFER FUNCTION PRODUCTS

Figure 30. Transfer function products.

2. COMPARISON OF SIMPLE MODELS

The first comparison of HEMP and lightning to be presented uses the simple models of the slab model (Section III, paragraph 4a) for HEMP and the simple continuity of current model (Section III, paragraph 5) for lightning. In Figure 31, the two models are used to compare the surface magnetic field, on a 1 m radius cylinder, generated by HEMP and by direct strike lightning. HEMP is calculated from the incident waveform in Equation 2 with a peak field of 60 kV/m, as the saturation field. The surface magnetic field is then doubled to account for reflection. Direct strike lightning is calculated using the continuity equation (Eq. 7) with the reasonable worst case current of 100 kA. A moderate threat waveform may be found by using the Fourier transform of Equation 7 with a peak current of 10 kA, but with the same 10^{11} A/s peak rate of

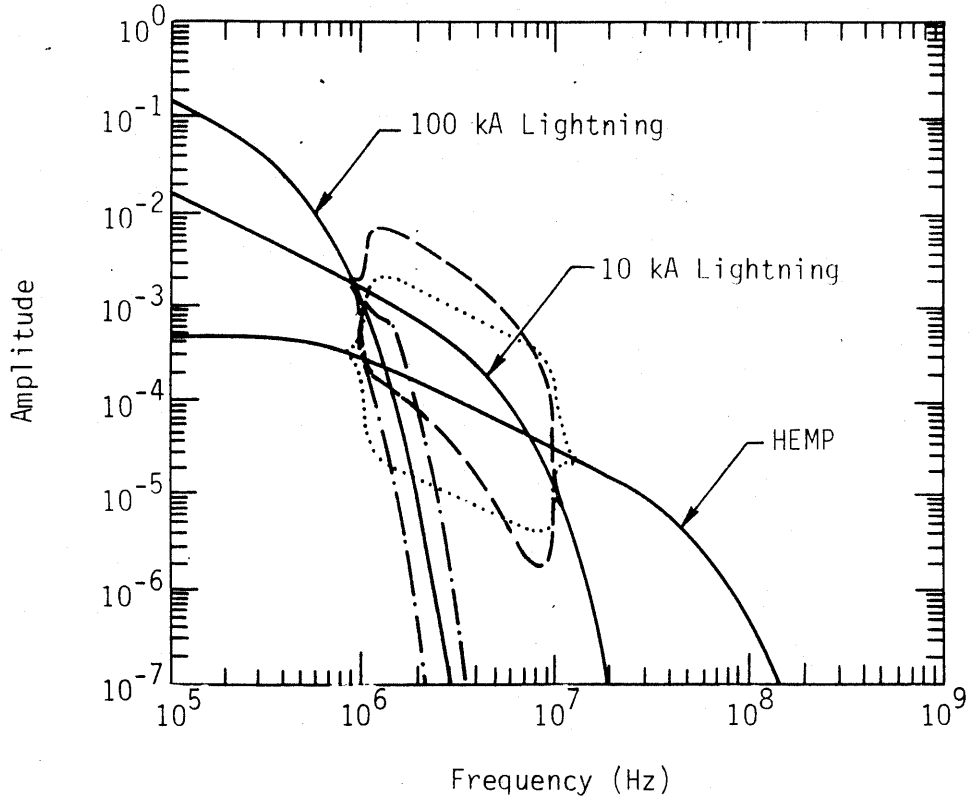

Figure 31. Spectrum of H for two waveforms for direct strike lightning and for HEMP. The uncertainty envelopes show the effect of the resonant region.

rise as the reasonable worst case current. This spectrum is also shown in Figure 31.

From these graphs, a different conclusion is apparent for the three frequency bands: 1) subresonant, 2) resonant, and 3) superresonant. Below about 1 MHz, the lightning threat is clearly dominant. In this spectral region, lightning is far more likely to cause physical damage to the aircraft or to penetrate the aircraft by diffusion than HEMP. Within the resonant region, (described in Section IV, paragraph 1) it is not clear which threat dominates. However, above 10 MHz or so, HEMP is much larger. Significantly, this indicates that apertures, even smaller than those required for adequate protection against lightning, must be considered when hardening aircraft against HEMP.

Figure 31 reveals a singular feature of the double exponential function of Equation 2. The high frequency characteristics of this function are uniquely determined by the value of the rate of rise of the function which occurs at $t = 0$. For the reciprocal double exponential this is not true since the high frequency fall off is exponential rather than $1/f^2$. For this reason the moderate threat, when described by the reciprocal double exponential, actually is a more severe threat at high frequencies than the reasonable worst case threat, as described by the reciprocal double exponential.

Clearly, the two threats as described by these simple models are different; each requires that a different hardening technique be developed in order to adequately protect aircraft.

Only the surface current is compared in this comparison of simple models since calculating even a first order estimate of the charge requires a finite length model.

3. MORE COMPLEX MODELS

Since the models used in the comparison above are very simple and since the electromagnetic response of aircraft to actual lightning and HEMP threats

is very complicated, an illustration of more complicated analysis techniques is needed. While the two methods used in the comparison below are still very simple compared to the phenomena of the real interactions they attempt to model, they represent a more complete comparison than previously shown (Section IV, paragraph 2). In this section, the Sassman model (Ref. 46) determining the response of a finite length cylinder is compared to a transmission line model that assesses the response of a finite cylinder to an injected lightning current.

Figure 32 shows a comparison of the magnetic field strength H frequency components for the specified threat waveforms at the aircraft's surface. Since plots for linear current density (A/m/Hz) and magnetic field are essentially the same, Figure 32 compares the net surface currents as well. The

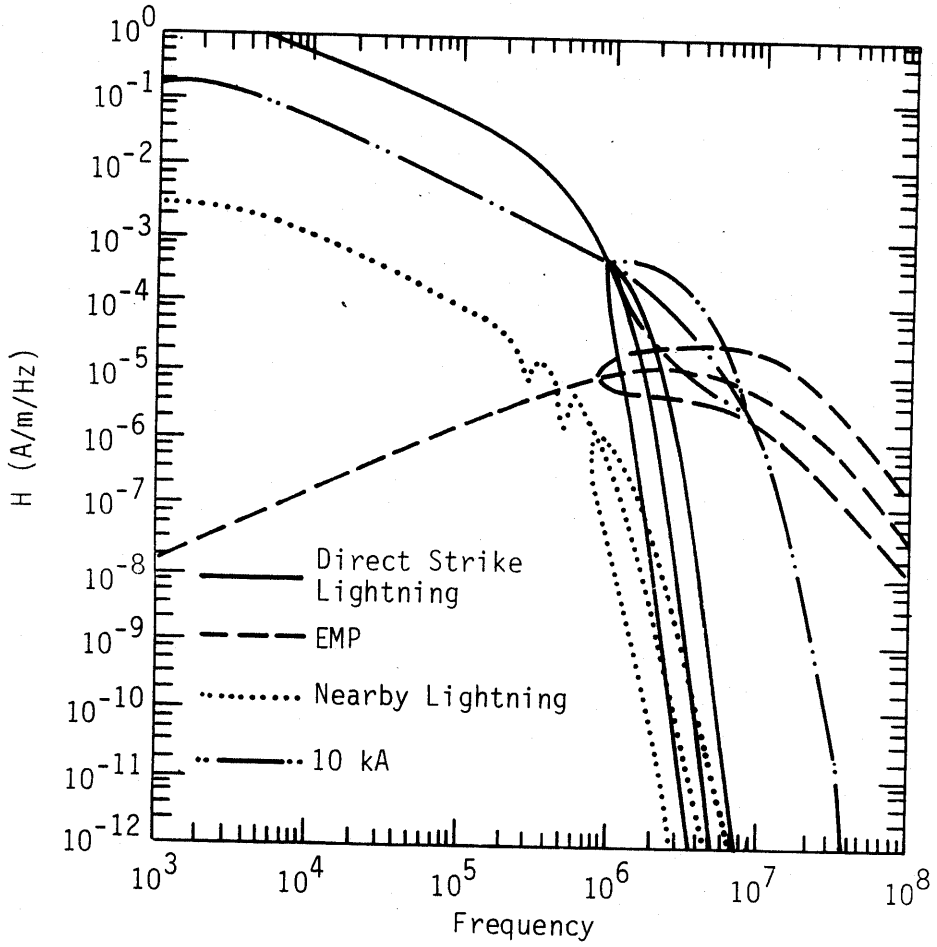

Figure 32. Comparison of magnetic field intensity H for HEMP and lightning using the more sophisticated models.

"sampling point" is one-fourth the distance from the nose to the fuselage; however, even if the point is varied, the spectrum is only marginally affected. The F-106B is assumed to be a 1 m radius cylinder in all cases. For the nuclear EMP case, the threat waveform is taken from simple formulas, (Ref. 61). If H is known, these simple formulas can give the other desired fields. Also, using MKS units, $B = \mu H$, and $E = Z_0 H$ for an electromagnetic wave, can yield the other fields. For both lightning cases, the reciprocal sum-of-exponentials given in Section I can be used for the current versus time behavior.

In Figure 33, a similar comparison is presented, but $D_{normal} = \sigma$, the surface charge density rather than the surface current as shown in Figure 32 is presented. The nearby strike and the direct strike lightning waveforms are computed using the transmission line model of Section III, paragraph 6 as was developed for Figure 32. The calculation of the charge on a cylinder with dimensions as above for HEMP was accomplished using a simple extension to the work of Sassman (Ref. 46) to include the calculation of surface charge using the continuity equation. In addition, the surface charge was calculated using a simple prolate spheroidal model (Ref. 61), with the eccentricity chosen to obtain agreement with the Sasssman type model.

4. CONCLUSIONS

The general conclusions, the results shown in Figures 32 and 33, then, are:

(1) For all frequencies of interest, a direct strike constitutes a far greater threat than a nearby lightning strike. Indeed, the latter may be generally ignored.

(2) Below a frequency of approximately 2 MHz, a direct strike is a greater threat for aircraft than HEMP; above this frequency, though, HEMP is the greater threat. Details of the HEMP and lightning threat models as well as the response models affect this conclusion only when the crossover frequency is changed.

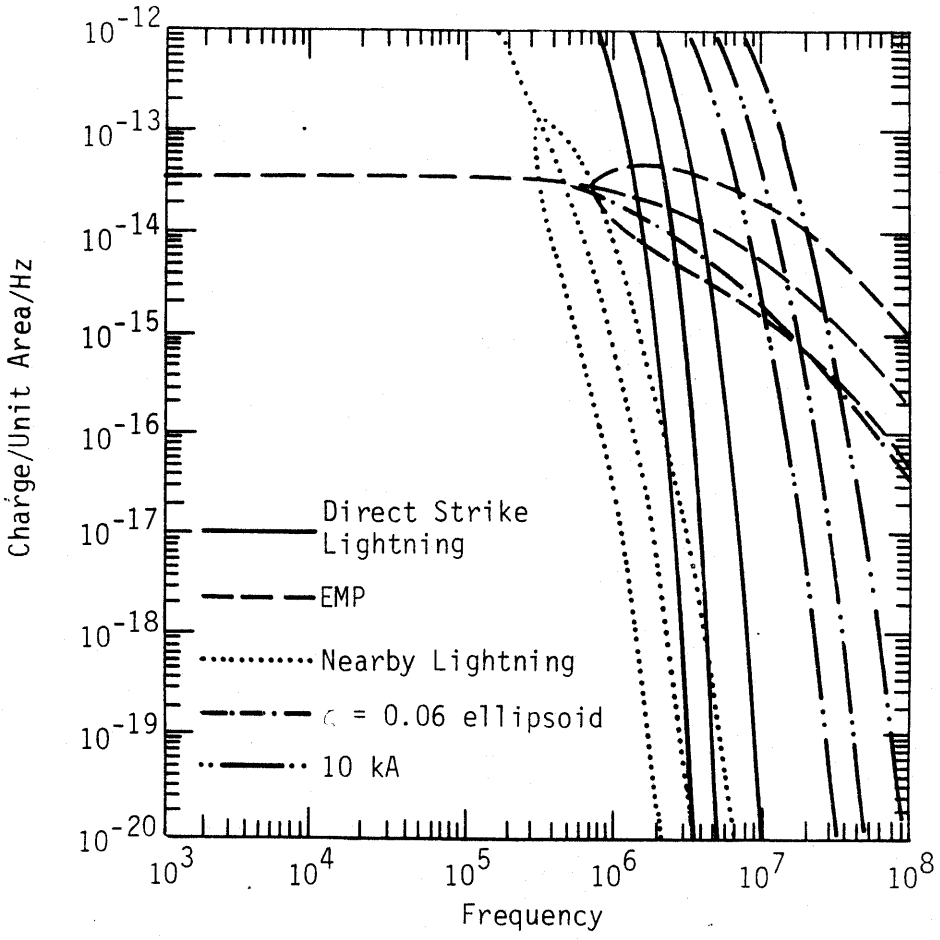

Figure 33. Comparison of the surface charge density for HEMP and lightning.

Since the direct strike currents effectively inhibit nearby strike effects, we may dismiss the latter from consideration. Although the results are approximate, it is clearly not possible to consider HEMP effects less severe than those of lightning.

Significantly, then, at the lowest frequencies, the lightning threat is more serious than the threat of HEMP. The reverse is true, however, for higher frequencies. Although the cross over point in frequency depends on the detailed assumptions of lightning currents and waveforms, etc., it is typically between 0.2 and 10 MHz; the latter value for the crossover point applies to a comparison for direct strike effects versus HEMP, while the former applies to a nearby strike.

V. OPERATIONAL ENVIRONMENTS

A comparison of HEMP and lightning is not complete without considering the differences in the operational environments for aircraft exposed to these two threats. In this final section, then, the differences in the way aircraft are operated in the presence of HEMP and lightning threats are described; and the differences in the way the probability of failure data can be interpreted for the two threats is assessed. This operational philosophy, of course, differs in wartime and peacetime. Although HEMP is exclusively a wartime threat, aircraft are susceptible to lightning strikes in both wartime and peacetime. Consequently, the hardening philosophy for lightning is based on peacetime operational experience and that for HEMP is based on postulated wartime scenarios. Consequently, a failure rate that is tolerated in peacetime for lightning cannot be tolerated during wartime for HEMP.

1. OPERATIONS IN A LIGHTNING ENVIRONMENT

Aircraft must be protected from lightning during the peacetime operational environment, that is, for training flights and normal cargo and passenger runs. During peacetime the schedules for these missions are not usually critical; therefore delays due to thunderstorm avoidance are regularly permitted and in most cases required. Such avoidance procedures help keep the incidence of reported lightning strike down to one in approximately 10^6 flight hours. Commercial aircraft have about an order of magnitude higher incidence of lightning strikes because of a stricter adherence to schedule (Ref. 62); consequently, a somewhat high incidence of lightning strikes to military aircraft might be expected during wartime.

If a strike occurs, there is a relatively high probability of an effect on mission accomplishment. The summary of the Air Force data base on lightning strikes given by Corbin (Ref. 63), shows that 37 percent of the reported lightning strikes resulted in at least a precautionary landing that became a mission abort. In less than 1 percent of the reported mishaps, there was a forced landing; additionally, in less than 1 percent of the mishaps, the aircraft was lost. As these data indicate, for each reported lightning strike

mishap there was: a 37 percent chance of a mission abort; less than 1 percent (0.8 percent chance from Ref. 63) chance of a forced landing; and less than 1 percent chance (0.8 percent chance from Ref. 63) of an aircraft loss. In addition, there is about an 8 percent probability of damage to system electronics. Experience for electrical outages for civilian aircraft is similar with 11 percent of 783 strike reports requiring ground crew maintenance of particular electronic components (Ref. 64). Coupled with the small probability of a mishap, approximately 10^{-6} per flight hour, these various degrees of mishap are rarely observed in peacetime.

Although, there are unreported strikes as well as damage to aircraft by lightning that have been attributed to other causes. Occurrence of a strike defined here is an actual report of a strike. However, the reported statistical base available for this study represents at least qualitatively the actual probability of a particular occurrence during a lightning strike.

2. OPERATION IN A HEMP ENVIRONMENT

A HEMP environment is experienced by an aircraft during wartime. In all probability an aircraft will experience HEMP environment at least once during each mission. In fact, some scenarios indicate that the Soviets may use multiple high altitude bursts; each burst would expose essentially all the aircraft within an area the size of the continental U.S. to HEMP. Significantly, unlike the relative complete data base for lightning, no statistics on the probability of a certain type of failure per HEMP exposure are presently available. However, the data base for lightning does provide some guidance for estimating the probability of failure per HEMP event.

For lightning, the damage to aircraft is skewed toward structural damage. Of 877 mishaps analyzed (Ref. 63), 78 percent reported structural damage and 8 percent reported damage to electronic components. Of course one should be cautious since the reported mishaps and damage are not necessarily complete. Since HEMP's peak frequency is higher than lightning's, it is expected that

HEMP would cause more damage to electronics than to the aircraft's structure. Since so many wartime missions depend on sophisticated electronics for accurate delivery of weapons, the effect on the fraction (that is, 37 percent for lightning) of missions aborted per event would not necessarily change.

3. SUMMARY

If 37 percent of the aircraft exposed to each HEMP event aborted its mission, the Air Force inventory would be quickly depleted with the expenditure of only a few nuclear weapons by an adversary. This argument holds for 37 percent mission abort or for the 8 percent rate of damage to electronic systems. Figure 34 summarizes the results for lightning. These statistics, however, are missing several important physical variables necessary for determining the probability of failure for lightning.

(1) Data is taken on a variety of systems so that the probability of failure for a given aircraft cannot be determined.

(2) Lightning varies considerably in intensity and waveform, so that there is a variation in threat environment for lightning.

(3) The system response is not necessarily proportional to the threat intensity, so that if the intensity of the threat is increased the degree of damage may increase drastically, if a threshold is exceeded.

Because of the differences in the way aircraft are operated in wartime and peacetime, hardening programs must be designed to ensure the survival of mission capable aircraft in both war and peace. Failure rates tolerated in peacetime for lightning, because threat exposure may be avoided, may not be tolerable in a wartime situation when such a threat environment may not be avoided.

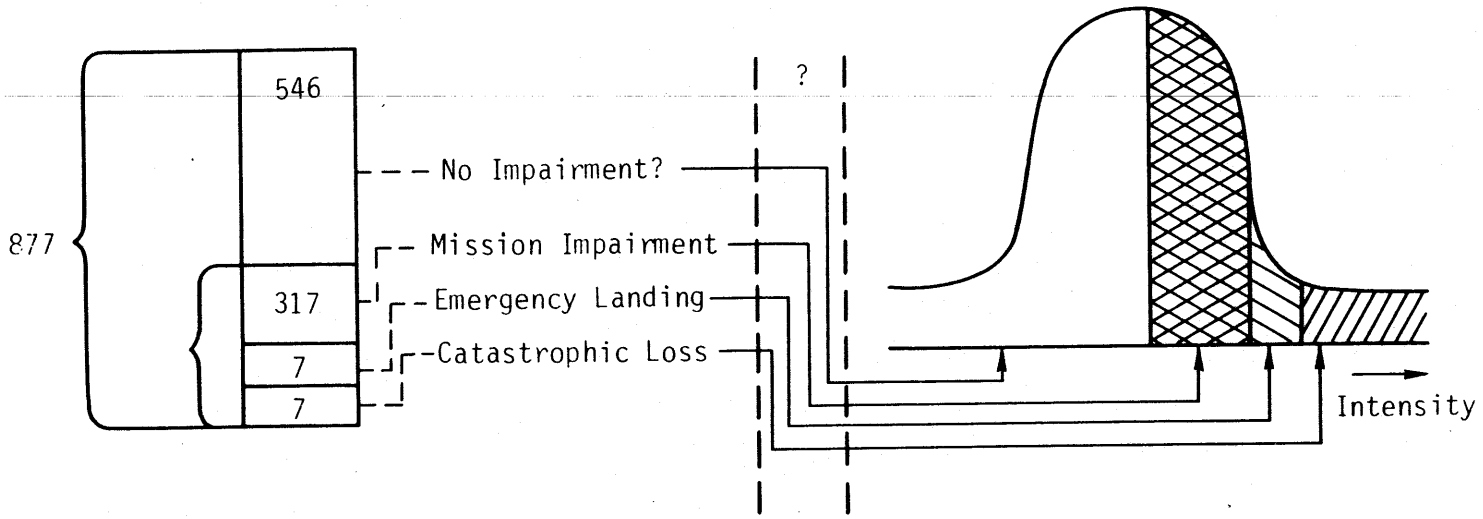

$$P_{MI/E} = P \text{ (Mission Impairment/Strike)} \simeq 0.37$$

Figure 34. Demonstration of probability of mission impairment from lightning data.

VI. CONCLUSIONS

In this report a number of different aspects of lightning and HEMP have been discussed. The electromagnetic environments were established for HEMP from Air Force documents and for lightning currents from available experimental data. The HEMP waveforms are described by a reciprocal double exponential; this form was chosen because of the waveform's exponential rise at very early time. The curve fit used a rise time constant of 2 ns (a 10-90 percent rise time of about 5 ns); a fall of 250 ns; and a peak field value of the saturated HEMP field, 60 kV/m. A similar reciprocal double exponential waveform is suggested after attempting to make experimental data fit a typical lightning return stroke current. While there are limited data available and a large span of lightning characteristics, the reciprocal double exponential with a peak rate of rise of 10^{11} A/s, a 50 μs duration and peak current of 100 kA forms an envelope for a reasonable worst case current waveform. The lightning current also radiates electromagnetic fields that interact with an aircraft in much the same way as HEMP. However, because the nearby strike interacts with an aircraft far less efficiently than the direct strike, the direct strike constitutes a more severe threat. Therefore, the direct strike was the basis for comparing the interaction of HEMP and lightning with aircraft.

Lightning and HEMP interact with aircraft differently because HEMP is an incident plane wave and because in direct strike lightning, current actually flows on the aircraft skin. For direct strikes, large charge densities appear at locations of small radii of curvature on the aircraft skin. Additionally, brush corona also exist near the regions as well as near the edges of apertures. For the return stroke, the attached channel responds to the current flowing through it in a nonlinear way because the narrow dimensions of channel make it resistive and inductive at early times; but at later times it becomes a good conductor.

When direct strike lightning and HEMP are compared in terms of the currents each produces on the surface of a finite length cylinder, and when

nonlinear effects are ignored, systematic differences are revealed. At frequencies lower than the resonances of the aircraft, the static region of the electromagnetic spectrum, lightning currents are much larger than those produced by HEMP. This low frequency dominance is demonstrated by the fact that lightning produces structural damage and HEMP generally does not. At frequencies above about 10 MHz, the higher frequency content of the generation mechanisms of HEMP causes the currents on the the test cylinder to be considerably larger than those of lightning in the same band. Between 1 and 10 MHz, the response of even a finite length cylinder is so complicated and so configuration dependent that neither threat is dominant across the band.

Because the responses of a cylinder to a plane wave and to current injection differ ultimately, and the threats differ significantly in different frequency regimes, each threat will require a different approach in order to sufficiently harden aircraft.

Finally, operational differences also require different approaches for hardening aircraft against HEMP or against lightning. Since lightning seldom strikes an aircraft (about once per million flight hours) a high failure rate per event can be tolerated. However of the reported lightning strikes, 37 percent resulted in mishaps ranging in severity from a precautionary landing to the loss of the aircraft. Since it is essentially certain that during war an aircraft will be exposed to HEMP at least once each mission, a similar abort rate would seriously erode fleet efficiency.

Since lightning and HEMP present different electromagnetic threats to aircraft, each requires a different hardening technique. By correctly assessing the ramifications of the threat and by developing hardening techniques tailored for each threat, researchers can ensure that advanced aircraft can successfully complete their missions in both peace and war.

REFERENCES

1. Taylor, C. D., "External Interaction: Coupling, Difference of Two Exponentials," in EMP Interaction Principles: Techniques, and Reference Data, K. S. H. Lee, editor, AFWL TR-80-402, Air Force Weapons Laboratory, Kirtland Air Force Base, NM, 1980.

2. Longmire, C. L., "The Physics of EMP," in EMP Interaction: Principles, Techniques and Reference Data, K. S. H. Lee, editor, AFWL TR-80-402, Air Force Weapons Laboratory, Kirtland Air Force Base, NM, 1980.

3. Vance, E. F., "Illustrative System Examples," EMP Interaction: Principles, Techniques, and Reference Data, K. S. H. Lee, editor, AFWL TR-80-402, Air Force Weapons Laboratory, Kirtland Air Force Base, NM 1980.

4. Longley, H. J. and C. L. Longmire, Development of the CHAP EMP Code, DNA 3150T, Defense Nuclear Agency, Washington, D.C., 1972.

5. Uman, M. A., Lightning, McGraw-Hill, New York, 1969.

6. Golde, R. H., "Lightning Currents and Their Parameters," in Lightning, Vol. I, Physics of Lightning, R. H. Golde, ed., Academic Press, London, 1977.

7. Trost, T. F. and F. L. Pitts, Analysis of Electromagnetic Fields on an F-106B Aircraft During Lightning Strikes, Proceeding of International Aerospace Conference of Lightning and Static Electricity, St. Catherine's College, Oxford, England, 23-25 March 1982.

8. Uman, M. A., Chapter 4, Lightning, McGraw-Hill, New York, 1969.

9. Garbagnati, E., et al., "Rilievi delle caralterishiche dei fulmine in Italia. Risultate ottenuti negli anni, 1970-1973.

10. Garbagnati, E., et al., "Lightning Parameters--Results of 10 Years of Systematic Investigation in Italy" in Proceedings of the International Aerospace Conference on Lightning and Static Electricity, Oxford, England, 23-25 March 1982.

11. Melander, B. G. and W. W. Cooley, Atmospheric Electricity Hazards Threat Environment Definition, Boeing Report No. 81205, The Boeing Military Airplane Company, Seattle, WA, 18 April 1983.

12. Garbagbati, E., "Experimental Measuring Stations for Investigation on Lightning Current and Thunderstorms," European Meeting of Lightning Instrumentation, 21-22 November 1975.

13. Baum, C. E., et al., Location of Lightning Electromagnetic Sources by Time of Arrival Compared to Inference from Electromagnetic Fields, Thunder Acoustics, and Videotape Photographs, Lightning Phenomenology Note 11, Lightning Phenomenology Notes, EMP Note Series, Air Force Weapons Laboratory, October 1983.

14. Rustan, P. L., et al., Airborne Lightning Characteristics, AFWAL TR-83-3013, Flight Dynamics Laboratory, AFWAL, Wright Patterson Air FOrce Base, OH, January 1983.

15. Pitts, Felix and M. E. Thomas, 1980 Direct Strike Lightning Data, NASA TM 81946, NASA Langley, February 1981.

16. Pitts, F. L. and M. E. Thomas, 1981 Direct Strike Lightning Data, NASA TM 83273, NASA Langley, March 1982.

17. Pitts, F. L. and M. E. Thomas, 1982 Direct Strike Lightning Data, NASA Technical Memorandum 84626, 1983.

18. Norinder, H. and O. Dahle, "Measurements by France Aerials of Current Variations in Lightning Discharges," Arkiv. Mat. Astron. Fysik, 32A, pp. 1-70, 1945.

19. Uman, M. A., D. K. McLain, and E. P. Krider, "The Electromagnetic Radiation from a Finite Antenna," Amer. J. Phys., 43, 33-38, 1975.

20. Lin, Y. T., M. A. Uman, and R. B. Standler, "Lightning Return Stroke Models, J. Geophys. Res. 85, pp. 1571-1583, 1980.

21. Master, M. J., et al., "Calculations of Lightning Return Stroke Electric and Magnetic Fields Above Ground," J. Geophys. Res. 86, 12127-12132, 1981.

22. Uman, M. A., M. J. Master, and E. P. Krider, "A Comparison of Lightning Electromagnetic Fields with the Nuclear Electromagnetic Pulse in the Frequency Range 10^4-10^7 Hz," IEEE Trans. EMC, EMC-24, No. 4, November 1982.

23. Jordan, D. J. and M. A. Uman, "Variations in Light Intensity with Height and Time from Subsequent Return Strokes," EOS Trans. AGU, 61, p. 977, 1980.

24. Uman, M. A., Lightning, p. 7, McGraw-Hill, New York, 1969.

25. Berger, K., "The Earth Flash" in Lightning I. Physics of Lightning, R. H. Golde, editor, Academic Press, p. 175, 1977.

26. Boyle, J. S. and R. E. Orville, J. Geophys. Res. 81, 4961, 1976.

27. Krider, E. P. and E. D. Weidman, "The Submicrosecond Structure of Lightning Radiation Fields," in Proceedings of the 8th International Aerospace and Ground Conference on Lightning and Static Electricity, DOT/FAA/CT-83/25, Federal Aviation Administration, Technical Center, Atlantic City Airport, NJ.

28. Plooster, M. N., "Numerical Simulation of Spark Discharge in Air," Phys. Fl., 14, pp. 2111-2123.

29. Braginskii, S. I., "Theory of the Development of a Spark Channel," J. Exptl. Theoretical Phys. (USSR), 34 1548-1557, 1958.

30. Uman, M. A., "The Diameter of Lightning," J. Geophys. Res., 69, 583-585, 1964.

31. Plooster, M. N., "Numerical Model of the Return Stroke of the Lightning Discharge," Phys. Fl. 14, 2124, 1971.

32. Ramo, S., J. R. Whinnery, and T. Van Duzan, Fields and Waves in Communication Electronics, Wiley, New York, 1967.

33. Golde, R. H., "Lightning Currents and Their Parameters," in Lightning, Vol. I, Physics of Lightning, R. H. Golde, ed., Academic Press, London, p. 179, 1977.

34. Baños, A., Dipole Radiation in the Presence of a Conducting Halfspace, Pergamon, Oxford, 1966.

35. Krider, E. P. and E. D. Weidman, "The Submicrosecond Structure of Lightning Radiation Fields" in 8th International Aerospace and Ground Conference on Lightning and Static Electricity, DOT/FAA/CT-83/25 Conference Publication, June 1983.

36. Baum, C. E., E. L. Breen, J. P. O'Neil, C. B. Moore, and D. L. Hall, Measurements of Electromagnetic Properties of Lightning with 10 Nanosecond Resolution, Lightning Phenomenology Notes, Note 3, February 1982.

37. Cianos, N. and E. T. Pierce, A Ground-Lightning Environment for Engineers Usage, Project 1834, Stanford Research Institute.

38. Baum, C. E. and R. L. Gardner, An Introduction to Leader Tip Modeling, Lightning Phenomenology Notes, Note 5, Air Force Weapons Laboratory, Kirtland Air Force Base, NM, 1983.

39. Baum, C. E. and L. Baker, Return Stroke Transmission Line Model, Lightning Phenomenology Notes, Air Force Weapons Laboratory, Kirtland Air Force Base, NM, 1983, to be published.

40. Albright, N. W and D. A. Tidman, "Ionizing Potential Waves and High-Voltage Breakdown Streamers," Phys. Fl. 15, p. 86-89, January 1972.

41. Corn, P. B., "Lightning Hazards Overview--Aviation Requirements and Interests," Proceeding-Workshops on the need for lightning observations from space, NASA Conference Publication CP-7095, NASA-Marshall Space Flight Center, AL.

42. EMP Note Series, C. E. Baum, ed., Air Force Weapons Laboratory, Kirtland Air Force Base, NM.

43. Meek, J. M. and J. D. Craggs, ed., Electrical Breakdown in Gases, John Wiley, Chichester, UK, 1978.

44. Baum, C. E., Simulation of Electromagnetic Aspects of Lightning, Lightning Simulation Notes, Note 1, February 1980.

45. Wilton, D. R., "Propagation--Low and Intermediate Frequencies," in EMP Interaction: Principles, Techniques, and Reference Data, K. S. H. Lee, editor, AFWL TR-80-402, Air Force Weapons Laboratory, Kirtland Air Force Base, NM, 1980.

46. Sassman, R. W., EM Pulse Interaction, Interaction Note 11, EMP Note Series, Air Force Weapons Laboratory, Kirtland Air Force Base, NM, 1967.

47. LeVine, D. M. and R. M. Meneghini, "Electromagnetic Fields Radiated From a Lightning Return Stroke: Application of an Exact Solution to Maxwell's Equations," J. Geophys. Res. 83, No. C5, 2377-2384.

48. Gardner, R. L, "Effect of the Propagation Path on Lightning-Induced Transient Fields," Radio Science, 16, pp. 377-389, May-June 1981.

49. Felsen, L. B., Transient Electromagnetic Fields, Springer-Verlag, Berlin, 1976.

50. Felsen, L. B. and N. Marcwvoritz, Radiation and Scattering of Waves, Prentice-Hall, Englewood Cliffs, NJ, 1973.

51. Mittra, R. and Y. Rahmat-Samii, "A Spectral Domain Analysis of High Frequency Diffraction Problems," in Electromagnetic Scattering, D. E. Uslenghi, ed., Academic Press, New York, NY, 1978.

52. Stratton, J. A., Electromagnetic Theory, McGraw-Hill, p. 209, New York, NY, 1941.

53. Taylor, C. D. and T. T. Crow, "Calculation of Natural Resonances for Perpendicular Crossed Wires Parallel to an Imperfect Ground," Electromagnetics, 3, pp. 41-64, 1983.

54. Lin, C. A. and J. T. Cordaro, "Determination of the SEM Parameters for an Aircraft Model from the Transient Surface Current," Electromagnetics, 3, pp. 65-75, 1983.

55. Baum, C. E., T. K. Liu, and F. M. Tesche, "On the Analysis of General Multiconductor Transmission-Line Networks," Interaction Note 350, Novembr 1978.

56. King, R. W. P., Transmission Line Theory, Dover, New York, NY, 1956.

57. Gunston, B., Modern Military Aircraft, Salamander, London, England, 1977.

58. Giri, D. V., R. S. Noss, D. B. Phnoc, and F. M. Tesche, Analysis of Direct and Nearby Lightning Strike Data for Aircraft, NASA Contractor Report 172127, LuTech, Inc., Contract NAS1-16893.

59. Turner, C. D. and T. F. Trost, Laboratory Modeling of Aircraft-Lightning Interactions, Final Report, NASA Grant NAG-1-28.

60. Endsley, D., et al., HPD Upgrade Testing Program Characterization Report, AFWL TR-78-251, Vol. II, Part 2, Air Force Weapons Laboratory, Kirtland Air Force Base, NM, 1978.

61. EMP Interaction: Principles, Techniques, and Reference Data, K. S. H. Lee, editor, AFWL TR-80-402, Air Force Weapons Laboratory, Kirtland Air Force Base, NM, 1980.

62. Nanevicz, T. E. and J. M. Hamm, Lightning and EMP Interaction with Aircraft, SRI Report T82-004.

63. Corbin, J. C., "Lightning Interaction with Aircraft," in 8th International Aerospace and Ground Conference on Lightning and Static Electricity, DOT/FAA/CT-83125 Conference Publication, June 1983.

64. Rasch, N. O., M. S. Glynn, and J. A. Plumer, "Lightning Interaction with Commercial Air Carrier Type Aircraft," in International Aerospace and Ground Conference on Lightning and Static Electricity, June 1984.

☆U.S. GOVERNMENT PRINTING OFFICE: 1984—576-142/10003